# MICROPROCESSOR CONTROLLED STATIC SLIP POWER RECOVERY SCHEME

## A DISSERTATION

*submitted in partial fulfilment of the*
*requirements for the award of the degree*
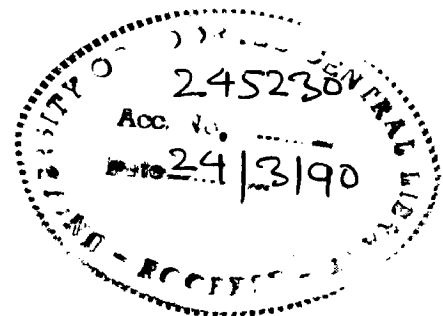*of*
MASTER OF ENGINEERING
*in*
ELECTRICAL ENGINEERING
(Power Apparatus and Electric Drives)

By

## VINOD KUMAR PANDEY

DEPARTMENT OF ELECTRICAL ENGINEERING
UNIVERSITY OF ROORKEE
ROORKEE-247 667 (INDIA)
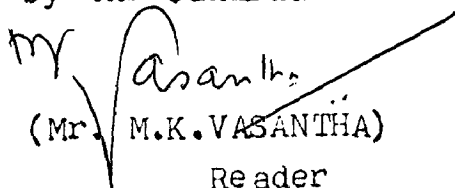
SEPTEMBER, 1989

# CANDIDATE'S DECLARATION

I hereby certify that the work which is being presented in the dissertation entitled MICROPROCESSOR CONTROLLED STATIC SLIP POWER RECOVERY SCHEME, in partial fulfilment of the requirement for the award of the degree of Master of Engineering in Electrical Engineering, University of Roorkee, Roorkee, is an authentic record of my own work carried out over a period of 36 months from Sept. 1986 to Sept. 1989 under the supervision of Dr. S.P.Gupta, Reader and Shri M.K.Vasantha, Reader, Department of Electrical Engineering, University of Roorkee, Roorkee, India.

The matter embodied in the dissertation has not been submitted by me for the award of any other degree or diploma.

DATED  SEPT.07 ,1989

(VINOD KUMAR PANDEY)

This is to certify that the above statement made by the candidate is correct to the best of our knowledge.

(Mr. M.K.VASANTHA)
Reader
Dept. of Electrical Engg.
University of Roorkee,
Roorkee-247667, India

(Dr. S.P.GUPTA)
Reader
Dept. of Electrical Engg.
University of Roorkee,
Roorkee-247667, India

# ACKNOWLEDGEMENT

I am also thankful to Sri K.K.Garg, Ex.Engg,

Sri S.P.Pandey, Sr. A.E., U.P.S.E.B., Azamgarh for

their unfailing inspiration and encouragement during

the completion of this work

Thanks are also due to Sri D.C.Bhardwaj for

typing the thesis in a short span of time.

(VINOD KUMAR PANDEY)

# ABSTRACT

The dissertation concerns the design, fabrication and evaluation of steady state performance of a micro - processor controlled static slip power recovery drive by using rectifier-line commutated inverter combination in the recovery loop. An idealized mathematical model describing the behaviour of the system has been developed based on the concept of coupled circuit approach. The system has been analyzed in synchronously rotating reference frame. The model involves the parameters which can be easily measured at the terminals of the slip ring induction motor. The equations describing steady state performance of the drive are derived from the general mathematical model.

The firing pulses for thyristors of the LCI are generated by the microprocessor in proper sequence with the help of synchronizing signals derived from supply voltage. The steady state performance has been obtained experimentally using the fabricated system and the experimental results have shown a good correlation with computed results.

# LIST OF SYMBOLS

| | |
|---|---|
| $V$ | instantaneous value of voltage |
| $i$ | instantaneous value of current |
| $V_{sm}$ | peak value of stator phase voltage |
| $R_{ss}$ | stator Resistance per phase |
| $R_{rr}$ | rotor Resistance per phase |
| $R_F$ | Resistance of d.c. link inductor |
| $L_F$ | inductance of d.c. link inductor |
| $L_{12}$ | mutual inductance between stator and rotor |
| $L_{ss}, X_{ss}$ | self inductance and reactance respectively of stator |
| $L_{rr}, X_{rr}$ | Self inductance and reactance respectively of rotor |
| $a$ | stator to rotor turns ratio |
| $a_T$ | recovery loop auto transformer turns ratio (inverter to mains side) |
| $L_M$ | $a\, L_{12}$ |
| $s$ | per unit slip |
| $p$ | differential operator, $\dfrac{d}{dt}$ |
| $P$ | Number of poles |
| $\omega$ | electrical angular speed corresponding to fundamental component of the applied voltage |
| $\omega_r$ | electrical angular speed of the drive |
| $T_e$ | electromagnetic torque |
| $\alpha$ | firing angle of the inverter |

## Subscripts

| | |
|---|---|
| a,b,c | phase quantities |
| d | direct axis quantities |
| q | quadrature axis quantities |
| s | stator quantities |
| r | rotor quantities |
| R | d.c. link quantities |
| I | inverter quantities |
| $f_b$ | supply feed back quantities |
| L | supply quantities |

# CONTENTS

Candidate's Declaration

Acknowledgement

Abstract

List of symbols

# CHAPTER - I

## INTRODUCTION

### .1.1    GENERAL

There is a growing demand for precise and reliable variable speed drive. The variable speed requirement has been met with d.c. motors. However, its commutator has always been a source of numerous troubles causing frequent break down of the drive. The brushes and commutator limits the maximum power of D.C.machine to 10 MW at 1000 RPM and makes it unsuitable for dusty and explosive environment.

The induction motor is a very attractive type of a.c. drive, because of its simple construction, ruggedness, low capital cost and absence of commutator problems. The speed control of induction motor may be accomplished by several methods, such as pole changing, pole amplitude modulation, stator voltage control, frequency control (variable frequency operation) and rotor resistance control. All of these methods suffer from one or other of the following disadvantages: excessive power loss in control, complicated control circuitry, high capital cost, lack of continuous variation in speed etc. A.C. commutator motors have also been used in past for achieving stepless speed control [1] but it is not so attractive, because of loss of the essential simplicity of induction motor.Commutator problems are more severe in this system as compared to d.c. drives. Despite the simplicity and economy of the induction

motor, its use as a variable speed drive has been limited until recently, because of high cost and complexity of the auxiliary equipment.

As a result of recent advances in solid state technology, the use of schemes employing stator voltage control, frequency changing, rotor resistance control and slip power recovery are becoming more popular. The limitation of stator voltage control [2] are the limited subsynchronous speed range and unsuitability for constant torque operation. In frequency changing schemes commutation and triggering cir - cuitry are very complex [3]. Moreover, this system exhibits a large region of instability at low values of frequencies [4], thus making the system unsuitable for low speeds. The variation of speed by rotor resistance control [5] is very simple and reliable, but is very in-efficient. The slip power recovery scheme utilizes the slip power available at the slip rings instead of wasting it in external rotor resistance.

1.2  SLIP POWER RECOVERY SCHEME

The slip power recovery scheme is very attractive be - cause of good efficiency. The recovered slip power is either added to the main motor shaft itself or returned to the supply, resulting in constant horse power and constant torque drive respectively. In a constant power drive the slip power is rectified and supplied to an auxiliary d.c. motor that produces reinforcing torque on the induction motor shaft. The speed of the drive is controlled by varying the excitation of the auxiliary d.c.motor. In a constant torque drive the slip

frequency of the recovered power is first converted to
supply frequency and then the recovered power is retur-
ned to the supply. Control of the speed is achieved by
changing the firing angle of the line commutated inver-
ter in the recovery loop.

1.3 LITRATURE SURVEY

Extensive litrature is available on slip power
recovery drive. Shepherd and Stanway [6] have experimen-
taly studied the steady state behaviour of the system.
The study has been carried out (1) by returning the recovered
energy direct to the supply (line feed back) and (2) by
feeding back the recovered power to auxiliary windings
on stator of slip ring induction motor. They have conclu-
ded that the drive exhibits the characteristics similar
to that of a separately excited d.c. motor. They have shown
that the speed regulation is better than stator voltage
control or rotor resistance control. Line feedback is highly
efficient with poor power factor and causes nonsinusoidal
supply current. Stater feedback improves the power factor
but has a poor efficiency at low speeds. Experimental inves-
tigation on capacitive compensation carried out by Shepherd
and Khalil [7] reveals that such approach leads to an appre-
ciable improvement in power factor.

Theoretical studies of the steady state behaviour
have been carried out by Lavi and Polge [8] with the
help of simplified equivalent circuit of the system.
The torque developed is proportional to the fundamen-
tal compoment of the rotor current. They have brought-
out that the presence of the rectifier bridge in rotor
circuit causes harmonic currents in the rotor and stator
which produce harmonic torques in addition to the har -
monic torques already present in conventional operation.
Erlicki [9] has presented the drive with rotor supplied
by inverter operating at a frequency greater than supply
frequency i.e. motor works with slip greater than unity
so that rotor revolves against rotating field. Under above
conditions, the inverter is the power source of the drive
and part of the slip power is fed back from the stator to
networks. Inverter operates at a frequency exceeding that
of supply mains which greatly facilitates its design and
construction. Mittle, Venkatesan, Gupta [10]have analysed
the system in a synchronously rotating reference frame and
arrived at a conclusion that the scheme is well suited for
a speed range from forty percent to rated speed with consi-
derable improvement in efficiency without adversely affec-
ting the power factor. Gupta and Venkatesan [11] have
studied the switching transients in static scherbius dri-
ve and concluded that -

(i)     Switching angle directly influences the
        initial magnitude and polarity of the dc
        components of current transients which
        results in peak magnitude appearing at
        different instants for different swit-
        ching angles.

(ii)    The peak magnitude of the current tran-
        sients is independent of switching angle
        and occurs within two cycles. Torque tra-
        nsients are independent of switching angle.

(iii)   Firing angle influences the magnitude of
        currents and torque transients.

Haylander and Hallenius [12] have observed the perfor-
mance improvement of the system by replacing the six
pulse converter with twelve pulse. The twelve pulse
converter reduces the stator current harmonics torque
pulsations. Subrahmanyam and Surendran [13] have analy-
sed the rotor current waveform during commutation and
interlude period using iterative procedure. The study
reveals that the rotor current waveform depends upon
the slip frequency and the torque pulsations have strong
dependency upon rotor frequency. The stator currents are
sinusoidal with superimposed slip dependent harmonics.
Olivier Stefanovic and April [14] have studied the sys-
tem with three different line commutated bridges (i.e.

six thyristor bridge, seven thyristor bridge and eight thyristor bridge) separately and compared their performances with respect to input power factor, efficiency total input current, size of d.c.link inductor and speed regulation. The best results are obtained with eight thyristors bridge. Drury, Jones and Brown [15] have utilized the concept of controlled freewheeling to recovery bridge and found improved performance with respect to reactive power consumption, system efficiency and power factor. Taniguchi, Takeda and Hirasa [16] have presented a modified slip power recovery scheme to overcome the disadvantages of conventional static slip power recovery drive. In this method slip voltage is rectified by diode bridge and stepped up with chopper and then with the help of PWM inverter is fed back to supply mains. The recovery current is converted into a sinusoidal waveform and the power factor of the drive can be adjusted to arbitrary values. Bose [17] has reviewed the technological status of adjustable speed A.C drives and covered almost all types of drives.

Mittle, Venkatesan, Gupta [18,19] conducted the stability analysis of constant torque slip power recovery drive and concluded that the unstable regions are present at low values of moment of inertia, over a certain range of firing angle and torque. The region of instability in-

creases with an increase in applied voltage. They claim that for normal values of inertia encountered in practice, the drive is stable over complete operating range.

Surendran and Subrahmanyam [20] recently analysed the system with the help of eigen value analysis for stability of drive in subsynchronous operation. They have found that the drive is stable in its entire operating range, even large variations in parameters do not produce instability. They have carried out the transient analysis of the system for step changes in torque at certain operating points described as unstable by Mittle and others [18-19], and found that system reaches the new steady state within a reasonable times. It is also concluded that the system damping increases with increasing firing angle of inverter. A root locus study of the system revealed that the system can become unstable only if the value of inertia constant is reduced below 1 % of its actual value, which is impossible in practice and thus the system is highly stable one. Regenerative braking in slip power recovery systems has been studied by Bird and Mehta [21] and by Bland and Shephered [22].

Tang, P.C., Lu, S.S. and Wu,Y.C. [23] have given a novel microprocessor controlled firing scheme for

three-phase full-wave thyristor dual converter. The range of firing angle control is from $0^{\circ}$ to $180^{\circ}$. The scheme utilizes minimum components without any adjustment and hence is highly reliable.

## 1.4 SCOPE OF PRESENT WORK

In the present work an attempt has been made to compute the steady state performance of constant torque slip power recovery drive and to experimentally verify the same with digital firing scheme using microprocessor. The present work has the following ob - jectives -

(i) To develop a mathematical model of the constant torque slip power recovery drive.

(ii) To compute the steady state performance using mathematical model.

(iii) Design and fabrication of converter inverter power circuit.

(iv) Development of microprocessor based firing scheme for line commutated inverter.

(v) To experimentally obtain the various performance curves from the fabricated system and compare the same with computed performance.

## 1.5 PRINCIPLE OF OPERATION OF CONSTANT TORQUE
## SLIP POWER RECOVERY DRIVE

The block diagram for constant torque slip power recovery drive is given in Fig. 1.1. The main components of a constant torque static slip power recovery drive are, a 3-phase rectifier bridge, filter circuit and a 3 phase line commutated inverter. Slip frequency rotor voltages are rectified by a 3-phase full wave diode bridge. The filter circuit smoothens the current undulations. The smooth direct voltage thus obtained constitutes the input to a 3-phase synchronous inverter, which operating in its invertering mode, returns energy to the supply mains at a rate depending upon the supply voltage, direct input voltage and the thyristor firing angle. The efficiency of this system is good because most of the slip power is fed back to the a.c. source. However a good efficiency is achieved at the cost of power factor, which becomes poor at low speeds of operation. The inverter used being line commutated, its circuitry is quite simple, which results in a low capital cost of the drive. Hence this system is becoming more popular compared to other systems of speed control. Constant torque slip power recovery drive exhibits the characteristics of separately
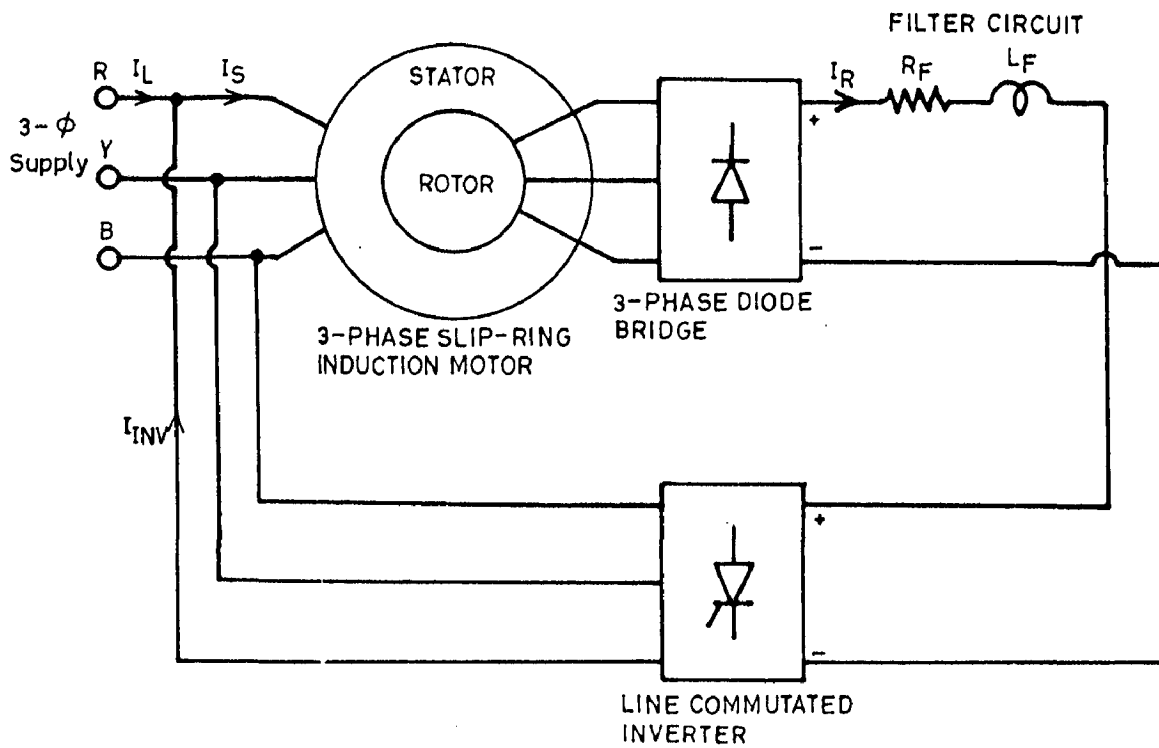
**Fig.1.1 :** Block diagram of constant torque slip power recovery scheme.

excited d.c. motor. The possible applications of
the proposed system are centrifugal pumps, fans,
hoists, cranes etc. The drive can be realised in
very high capacity (20 MW) because of inherent high
efficiency and can operate upto a speed of 3000 r.p.m.

# CHAPTER - II

## DEVELOPMENT OF MATHEMATICAL MODEL

## 2.1 INTRODUCTION

Generalised equations describing the behaviour of
slip power recovery drive employing 3-phase uncontro -
lled rectifier bridge coupled with line commutated
inverter in the rotor circuit are developed based on
coupled circuit approach. The system has been analyzed
in a synchronously rotating reference frame • With the
help of d-q transformation of variables, the basic equa-
tions for the idealized 3-phase symmetrical induction
motor are developed. Expressions for average values of
3-phase uncontrolled rectifier and 3-phase line commuta-
ted inverter are also written down. The equations of
the complete drive are then derived from the equations
of 3-phase induction motor and from the equations which
predict the average values of the uncontrolled rectifier
bridge and LCI variables.

Schematic diagram of static slip power recovery
drive is shown in Fig. 2.1. In this scheme, the rotor
windings of the induction motor are connected to a slip
power recovery circuit consisting of a 3-phase full wave
uncontrolled diode bridge, a smoothing filter and a line
commutated inverter. Slip power is extracted from   the
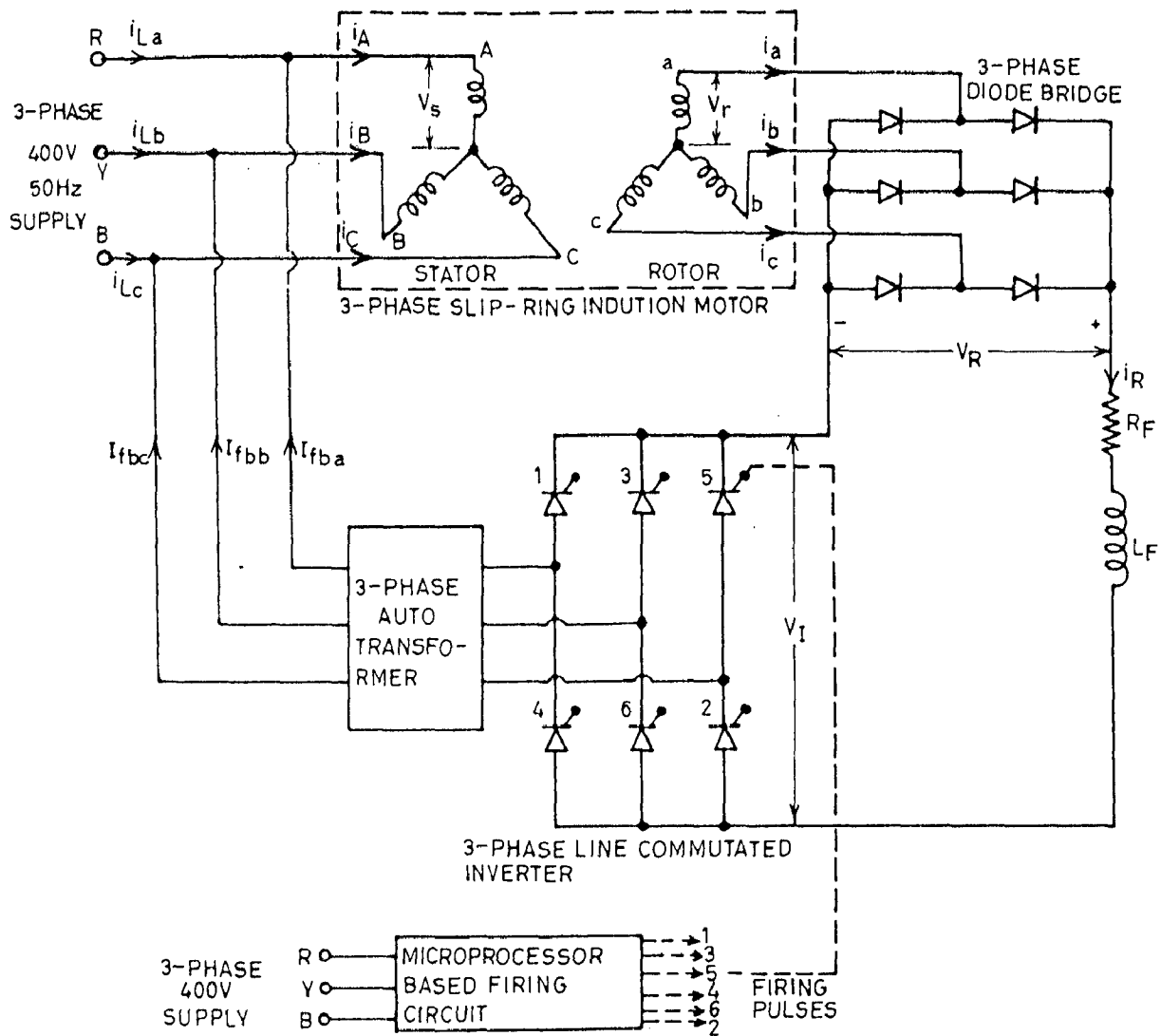
Fig.2.1: Schematic diagram of static slip-power recovery
drive.

rotor and returned to the supply at a rate fixed by the supply voltage and the inverter firing angle. The control of speed over sub synchronous motoring region from zero to rated speed is achieved by varying the firing angle of line commutated inverter. The mathe - matical model has been developed with following assumptions:

(i)     Saturation, hysteresis and eddy current effects in induction motor are neglected.

(ii)    Voltage drops in 3-phase uncontrolled diode bridge and LCI are neglected.

(iii)   Harmonics in induction motor rotor current and in the output current of the inverter are neglected.

2.2     ESTABLISHMENT OF BASIC EQUATIONS FOR THE DRIVE

2.2.1   Equations For 3-Phase Symmetrical Induction Motor

The generalised equations describing the behaviour of induction motor under transient and steady state conditions are established by considering it as an elementary two pole idealised machine [24-26]. The effect of no.of poles is taken into account by multiplying the expression for torque by number of pole pairs.

Schematic diagram of an ideal 3-phase symmetrical induction motor is shown in Fig. 2.2, wherein it is re-garded as a group of linear coupled circuits. Distri-buted stator and rotor windings have been shown by con-centrated coils. The magnetic axes of the individual stator and rotor phases have also been marked in Fig. 2.2 . The connections and current conventions for the stator and rotor phases are shown in Fig. 2.3 . Equa-tions for induction motor are established from the con-cept of generalised theory of machines. For the analy-sis of electromechanical devices, it is necessary to establish equations for both electrical and mechanical systems. Thus a mathematical formulation will have

(i)     a set of voltage- current equations,rela-ting the applied voltage to winding currents, using various circuit parameters.

(ii)    an equation of motion.

The induction motor voltage current equations in synchronously rotating d-q reference frame are [24-26].

$$
\begin{bmatrix} V_{ds} \\ V_{qs} \\ V_{dr} \\ V_{qr} \end{bmatrix} = \begin{bmatrix} (R_{ss}+L_{ss}p) & -\omega L_{ss} & L_{12}p & -\omega L_{12} \\ \omega L_{ss} & (R_{ss}+L_{ss}p) & \omega L_{12} & L_{12}p \\ L_{12}p & -s\omega L_{12} & (R_{rr}+L_{rr}p) & -s\omega L_{rr} \\ s\omega L_{12} & L_{12}p & s\omega L_{rr} & (R_{rr}+L_{rr}p) \end{bmatrix} \cdot \begin{bmatrix} i_{ds} \\ i_{qs} \\ -i_{dr} \\ -i_{qr} \end{bmatrix}
$$

...(2.1)
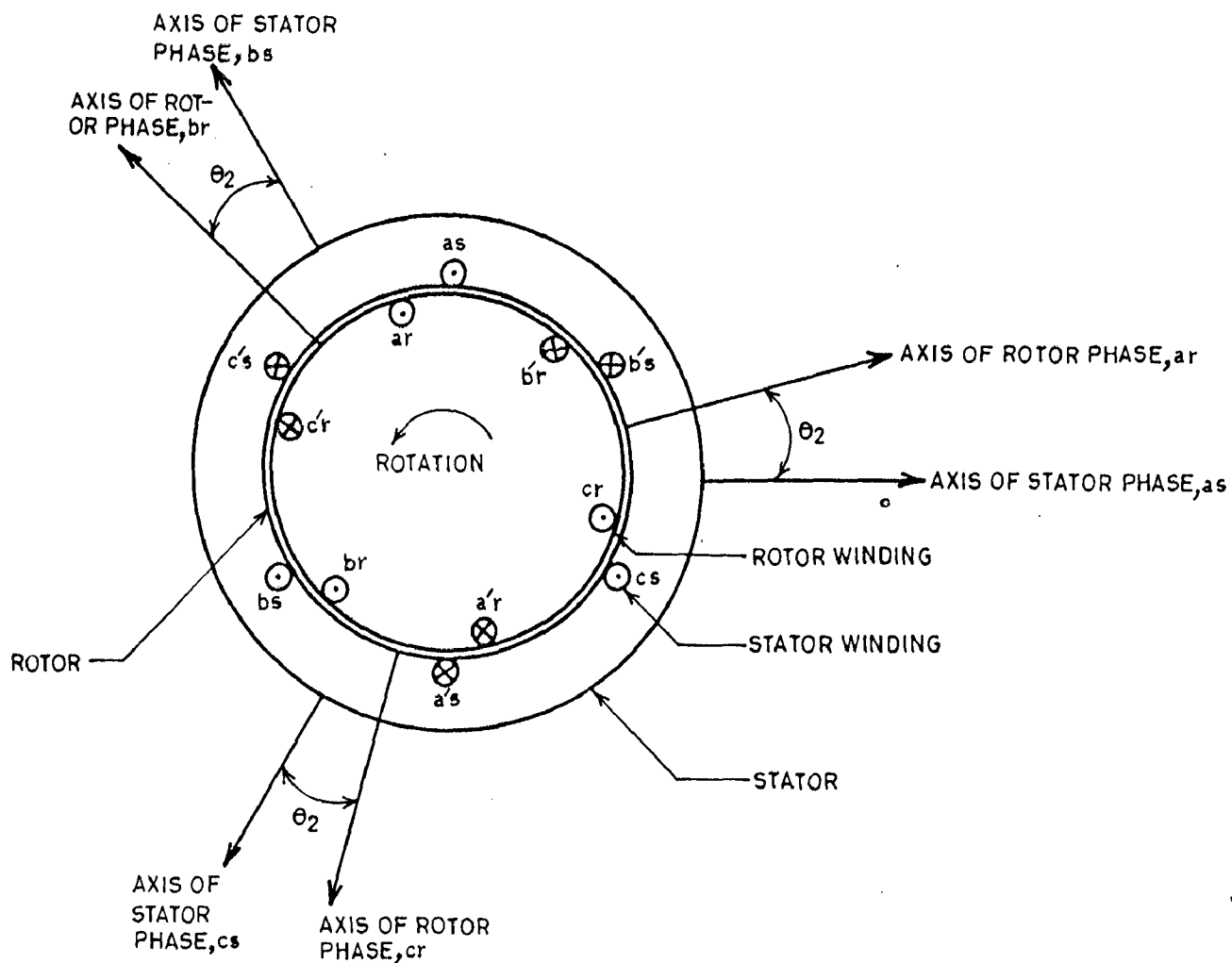
Fig. 2.2 : Idealized 3-phase symmetrical induction motor.
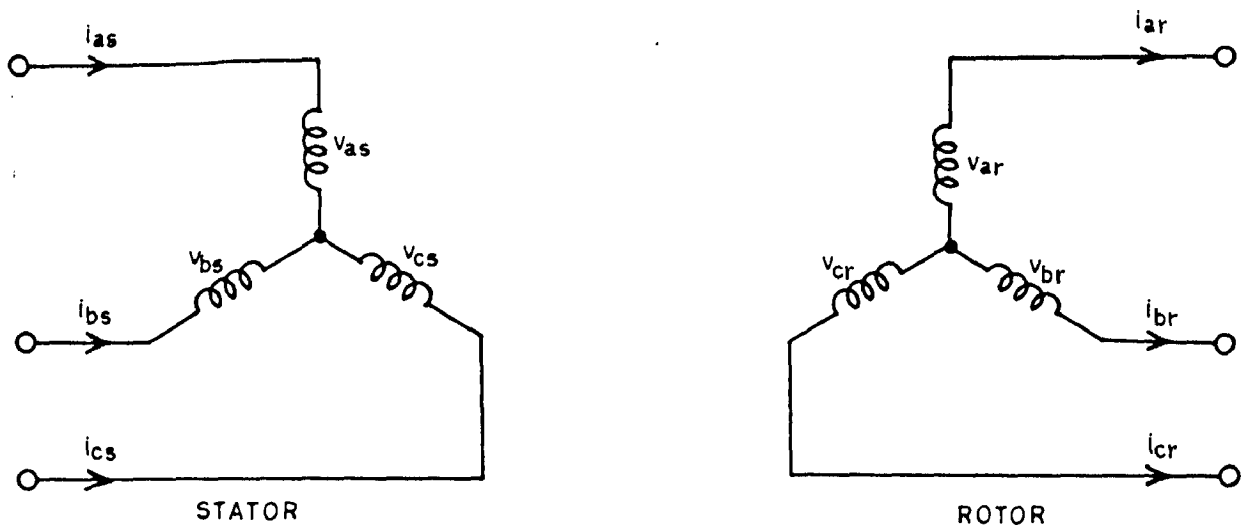
Fig. 2.3 : Connections and current conventions for 3-phase induction motor.



$$\dot{\theta} = \omega$$
$$\dot{\theta}_2 = \omega_r$$
$$\beta = \theta - \theta_2$$
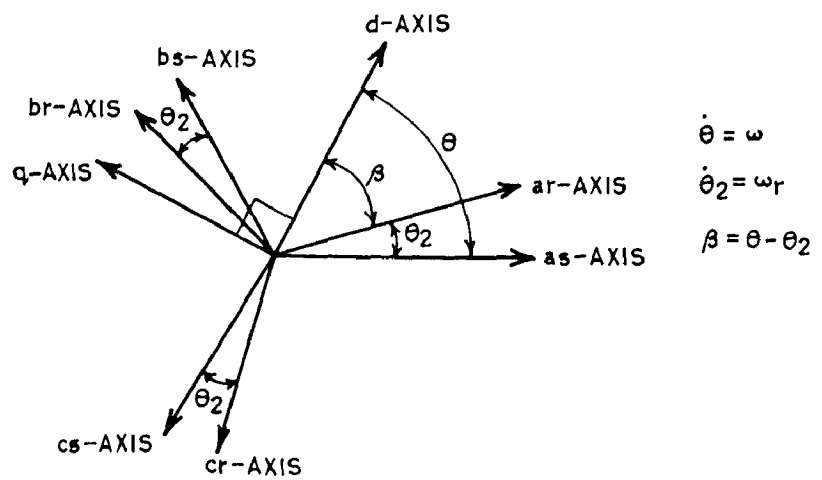
Fig. 2.4: Axis of 2-pole 3-phase symmetrical induction motor.

The electromagnetic torque developed by the induction motor in N-m is given by

$$T_e = \frac{3}{2} \frac{P}{2} L_{12} (i_{ds} i_{qr} - i_{qs} i_{dr}) \qquad ...(2.2)$$

where P is number of poles of induction motor. In writting above equations, conventional direction of power flow in the machine has been considered i.e. power flows into the motor at stator terminals and out of it at rotor terminals. Fig. (2.4) depicts the angular relationship of various axes of stator and rotor phases and those of synchronously rotating d-q reference frame, at any time t. Resolving phase voltages along d-q frame, the d-q voltages can be expressed as:

Stator

$$V_{ds} = \frac{2}{3} [V_{as} \cos \theta + V_{bs} \cos (\theta - \frac{2\pi}{3}) + V_{cs} \cos (\theta + \frac{2\pi}{3})]$$
$$...(2.3)$$

$$V_{qs} = -\frac{2}{3} [V_{as} \sin \theta + V_{bs} \sin (\theta - \frac{2\pi}{3}) + V_{cs} \sin(\theta + \frac{2\pi}{3})]$$
$$...(2.4)$$

Rotor

$$V_{dr} = \frac{2}{3} [V_{ar} \cos \beta + V_{br} \cos (\beta - \frac{2\pi}{3}) + V_{cr} \cos (\beta + \frac{2\pi}{3})]$$
$$...(2.5)$$

$$V_{qr} = -\frac{2}{3} [V_{ar} \sin \beta + V_{br} \sin (\beta - \frac{2\pi}{3}) + V_{cr} \sin (\beta + \frac{2\pi}{3})]$$
$$...(2.6)$$

where $\theta = \omega t$, $\beta$ = angle of advancement of d-axis w.r.t. axis of phase 'a' of rotor.

The choice of factor 2/3 is arbitrary.

If t=0 instant be so chosen that at this instant d-axis coincides with the stator 'as' axis and rotor 'ar' axis, then $\theta = \beta = 0$. Stator and rotor terminal voltages at any instant may be expressed as :

Stator

$$V_{as} = V_{sm} \cos \theta$$
$$V_{bs} = V_{sm} \cos (\theta - \tfrac{2\pi}{3})$$
$$V_{cs} = V_{sm} \cos (\theta + \tfrac{2\pi}{3}) \qquad \qquad \ldots(2.7)$$

Rotor

$$V_{ar} = V_{rm} \cos (\beta + \alpha_r)$$
$$V_{br} = V_{rm} \cos (\beta + \alpha_r - \tfrac{2\pi}{3})$$
$$V_{cr} = V_{rm} \cos (\beta + \alpha_r + \tfrac{2\pi}{3}) \qquad \qquad \ldots(2.8)$$

where $\alpha_r$ is an arbitrary phase angle, which is equal to the phase difference between stator and rotor phase voltages of a given phase at time zero.

Substituting from equations (2.7) and equations (2.8) in equation (2.3) to equation (2.6) ,

$$V_{ds} = V_{sm} \qquad \qquad \ldots(2.9)$$
and
$$V_{qs} = 0 \qquad \qquad \ldots(2.10)$$
$$V_{dr} = V_{rm} \cos \alpha_r \qquad \qquad \ldots(2.11)$$
and
$$V_{qr} = V_{rm} \sin \alpha_r \qquad \qquad \ldots(2.12)$$

2.2.2 Equation for Uncontrolled Bridge Rectifier

Assuming negligible ripple in the d.c. current at the rectifier output and neglecting voltage drop due to overlap, the average output voltage of a 3-phase uncontrolled rectifier bridge is given by [27].,

$$V_R = \frac{3\sqrt{3}}{\pi} V_{rm} \qquad \qquad ...(2.13)$$

where $V_{rm}$ is the peak value of fundamental phase voltage induced in the rotor.

Under the conditions, assumed above, the phase current at input to the rectifier is in the form of rectangular pulses of $\frac{2\pi}{3}$ duration, alternating at rotor frequency and having an amplitude of average d.c. current at the output i.e. $i_R$. The peak value of the fundamental component of phase current is therefore given by

$$i_{rm} = \frac{2\sqrt{3}}{\pi} i_R \qquad \qquad ...(2.14)$$

Fundamental power input to the rectifier is

$$P_{in} = 3 V_{ph} i_{ph} \cos \phi$$
$$= 3 . \frac{V_{rm}}{\sqrt{2}} \frac{i_{rm}}{\sqrt{2}} \cos \phi \qquad \qquad ...(2.15)$$

where $\phi$ is the phase angle between fundamental voltage and current of the rotor phase.

Power output from the rectifier is given by

$$P_{out} = V_R i_R \qquad \qquad ...(2.16)$$

Substituting equation (2.13) and (2.14) in equation (2.16)

$$P_{out} = \frac{3\sqrt{3}}{\pi} V_{rm} \cdot \frac{\pi}{2/3} i_{rm}$$

$$= 3 \cdot \frac{V_{rm}}{\sqrt{2}} \frac{i_{rm}}{\sqrt{2}} \qquad\qquad \ldots(2.17)$$

Assuming no losses in the rectifier, power input to the rectifier, should be equal to power output from rectifier.

or $3 \dfrac{V_{rm}}{\sqrt{2}} \dfrac{i_{rm}}{\sqrt{2}} \cos\phi = 3 \dfrac{V_{rm}}{\sqrt{2}} \dfrac{i_{rm}}{\sqrt{2}}$

so $\phi = 0^{\circ}$

It shows that fundamental component of rotor phase current is in phase with fundamental rotor phase voltage.

Therefore, the rotor phase currents can be expressed in accordance with the expressions(2.8), as

$$i_{ar} = i_{rm} \cos(\beta + \alpha_r)$$

$$i_{br} = i_{rm} \cos(\beta + \alpha_r - \frac{2\pi}{3})$$

$$i_{cr} = i_{rm} \cos(\beta + \alpha_r + \frac{2\pi}{3}) \qquad\qquad \ldots(2.19)$$

The transformation equation for rotor currents may be written as

$$i_{dr} = \frac{2}{3}[i_{ar}\cos\beta + i_{br}\cos(\beta - \frac{2\pi}{3}) + i_{cr}\cos(\beta + \frac{2\pi}{3})]$$

$$i_{qr} = -\frac{2}{3}[i_{ar}\sin\beta + i_{br}\sin(\beta - \frac{2\pi}{3}) + i_{cr}\sin(\beta + \frac{2\pi}{3})]$$

$$\ldots(2.20)$$

Substituting equations(2.19) in equations (2.20)

$$i_{dr} = i_{rm} \cos \alpha_r$$

$$i_{qr} = i_{rm} \sin \alpha_r \qquad \qquad \ldots(2.21)$$

## 2.2.3 Equation For Filter Circuit

The rectified voltage of uncontrolled bridge rectifier is smoothened by using a filter circuit and then applied to the LCI. The voltage equation of the filter circuit during continuous conduction ($i_R > 0$) may be written as follows

$$V_R = V_I + (R_F + L_F p) i_R \qquad \qquad \ldots(2.22)$$

## 2.2.4 Equation for Line Commutated Inverter

The LCI converts the smoothed d.c. voltage into a.c voltage of line frequency and returns, the slip power to the a.c. mains. Assuming infinitely smooth direct voltage and zero a.c. source impedance, the opposing e.m.f. presented by the inverter depends upon the firing angle, supply voltage and autotransformer turns ratio and is approximately equal to direct input voltage [27-28].

$$V_I = \frac{3\sqrt{3}}{\pi} a_T V_{sm} \cos (\pi - \alpha) \qquad \qquad \ldots(2.23)$$

where $V_{sm}$ is fundamental component of peak phase voltage at stator terminals and $a_T$ is auto transformer turns ratio (inverter side to mains side).

Substituting for $V_{sm}$ from equation (2.9) into equation (2.23).

$$V_I = \frac{3\sqrt{3}}{\pi} a_T V_{ds} \cos (\pi - \alpha) \qquad \ldots (2.24)$$

## 2.2.5 Equations of The Drive

Equations (2.1) can now be rewritten directly by substituting for $V_{ds}$ and $V_{qs}$ as $V_{sm}$ and 0 respectively. Substitution for $V_{dr}$ and $V_{qr}$ is done in following manner.

From equation (2.22) we have

$$V_R = V_I + (R_F + L_F p) i_R$$

Substituting for $V_R$, $V_I$ and $i_R$ from equations (2.13), (2.14) and equation (2.23) respectively.

$$\frac{3\sqrt{3}}{\pi} V_{rm} = \frac{3\sqrt{3}}{\pi} a_T V_{sm} \cos (\pi - \alpha) + (R_F + L_F p) \frac{\pi}{2/3} i_{rm}$$

or

$$V_{rm} = a_T V_{sm} \cos (\pi - \alpha) + \frac{\pi^2}{18} (R_F + L_F p) i_{rm}$$

$$\ldots (2.25)$$

Substituting for $V_{rm}$ from equation (2.11) into equation (2.25)

$$\frac{V_{dr}}{\cos \alpha_r} = a_T V_{sm} \cos (\pi - \alpha) + \frac{\pi^2}{18} (R_F + L_F p) i_{rm}$$

or

$$V_{dr} = a_T V_{sm} \cos \alpha_r \cos (\pi - \alpha) + \frac{\pi^2}{18} (R_F + L_F p) i_{dr}$$

$$\ldots (2.26)$$

Similarly by substitution from equation (2.12) into equation (2.25), we get

$$V_{qr} = a_T V_{sm} \cos (\pi - \alpha) \sin \alpha_r + \frac{\pi^2}{18} (R_F + L_F p) i_{qr}$$

$$\ldots (2.27)$$

Substituting for $V_{ds}$, $V_{qs}$, $V_{dr}$ and $V_{qr}$ in equations (2.1), the final voltage current equations of the drive are obtained as

$$
\begin{bmatrix}
V_{sm} \\
0 \\
a_T V_{sm} \cos(\pi-\alpha)\cos\alpha_r \\
a_T V_{sm} \cos(\pi-\alpha)\sin\alpha_r
\end{bmatrix}
=
\begin{bmatrix}
(R_{ss}+L_{ss}p) & -\omega L_{ss} & L_{12}p & -\omega L_{12} \\
\omega L_{ss} & (R_{ss}+L_{ss}p) & \omega L_{12} & L_{12}p \\
L_{12}p & -s\omega L_{12} & (R_{eq}+L_{eq}p) & -s\omega L_{rr} \\
s\omega L_{12} & L_{12}p & s\omega L_{rr} & (R_{eq}+L_{eq}p)
\end{bmatrix}
\cdot
\begin{bmatrix}
i_{ds} \\
i_{qs} \\
-i_{dr} \\
-i_{dr}
\end{bmatrix}
$$

$$\qquad \dots(2.28)$$

$$\text{where } R_{eq} = R_{rr} + \frac{\pi^2}{18} R_F \qquad \dots(2.29)$$

$$L_{eq} = L_{rr} + \frac{\pi^2}{18} L_F \qquad \dots(2.30)$$

and equation for the torque is given by

$$T = \frac{3}{2} \frac{P}{2} L_{12}(i_{ds} i_{qr} - i_{qs} i_{dr}) \qquad \dots(2.31)$$

Equations (2.28) contain five unknown variables i.e. $i_{ds}$, $i_{qs}$, $i_{dr}$, $i_{qr}$ and $\alpha_r$. They can be reduced to four by expressing $i_{dr}$ and $i_{qr}$ in terms of $i_{rm}$ and $\alpha_r$ from equations (2.21).

Generally the machine parameters are measured with respect to stator windings. Therefore it is more convenient to refer all the quantities to the stator windings. Hence referring all quantities to the stator winding, the final equations of the system are

$$
\begin{bmatrix} V_{sm} \\ 0 \\ aa_T V_{sm}\cos(\pi-\alpha)\cos\alpha_r \\ aa_T V_{sm}\cos(\pi-\alpha)\sin\alpha_r \end{bmatrix} = \begin{bmatrix} (R_{ss}+L_{ss}p) & -\omega L_{ss} & L_M p & -\omega L_M \\ \omega L_{ss} & (R_{ss}+L_{ss}p) & \omega L_M & L_M p \\ L_M p & -s\omega L_M & (R'_{eq}+L'_{eq}p) & -s\omega L'_{rr} \\ s\omega L_M & L_M p & -s\omega L'_{rr} & (R'_{eq}+L'_{eq}p) \end{bmatrix}
$$

$$
X \begin{bmatrix} i_{ds} \\ i_{qs} \\ -i'_{rm}\cos\alpha_r \\ -i'_{rm}\sin\alpha_r \end{bmatrix} \quad ..(2.32)
$$

where

$$
L_M = a\,L_{12} \qquad\qquad\qquad ...(2.33)
$$

$$
R'_{eq} = a^2 R_{eq} \qquad\qquad\qquad ...(2.34)
$$

$$
L'_{eq} = a^2 L_{eq} \qquad\qquad\qquad ...(2.35)
$$

$$
i'_{rm} = \frac{i_{rm}}{a} \qquad\qquad\qquad ...(2.36)
$$

$$
L'_{rr} = a^2 L_{rr}
$$

A prime is fixed to all referred quantities. Electromagnetic torque equation for the system may be expressed as

$$
T_e = \frac{3}{2}\,\frac{P}{2}\,aL_{12}\left( i_{ds}\frac{i_{qr}}{a} - i_{qs}\frac{i_{dr}}{a} \right)
$$

or

$$
T_e = \frac{3}{2}\,\frac{P}{2}\,L_M\left( i_{ds}\,i'_{qr} - i_{qs}\,i'_{dr} \right) \qquad ...(2.37)
$$

## 2.3 EQUATIONS OF DRIVE IN PER UNIT SYSTEM

It is advantageous to analyse the transient and steady state behaviour of the system based on a per unit system because of the following reasons.

(i) A simple inspection of the per-unit parameters immediately reveals much more about the basic nature of the machine than may be observed from ordinary parameters.

(ii) The numerical range of perunit parameters is small, which is valuable for solution by digital compu - ter.

(iii) Arbitrary numerical factors which may appear in the ordinary equations in d-q axes transformation are avoided.

The choice of base values for various quantities are made so that computational efforts are reduced. The base values chosen (Appendix-1) are defined as follows.

Unit voltage $= V_{base} =$ Peak value of rated phase voltage in volts $(V_{sm})$

Unit Current $= I_{base} =$ Peak value of rated phase current in Amps $(i_{sm})$

Unit Impedance $= Z_{base} = \dfrac{V_{base}}{I_{base}}$, ohms

Unit Power $= P_{base} =$ Rated apparent Power

$= \dfrac{3}{2} V_{sm} i_{sm}$ watts

Unit mechanical speed $= \)_{base} = \frac{2}{P} \omega$ rad/sec

Unit electrical speed $= \omega_{base} = \omega = 2\pi f = 100\pi$ rad/sec.

Unit Torque $= T_{base} = \frac{P_{base}}{base}$ N-m

Equations (2.32) can be converted in per unit form by dividing each quantity with their base value. Prime affixed to all refferred quantities may be withdrawn for simplification in handling the equations. First equation of equations (2.32) is given by

$$V_{sm} = (R_{ss}+L_{ss}p) \, i_{ds} - \omega L_{ss} \, i_{qs} - L_M p \, i_{dr} + \omega L_M \, i_{qr}$$

Dividing above equation by $V_{base}$

$$\frac{V_{sm}}{V_b} = \frac{(R_{ss}+L_{ss}p)}{V_b} i_{ds} - \frac{\omega L_{ss} \, i_{qs}}{V_b} - \frac{L_M p}{V_b} i_{dr} + \frac{\omega L_M}{V_b} i_{qr}$$

$$V_{sm}(p.u) = \frac{(R_{ss}+\omega L_{ss} \frac{p}{\omega})}{\frac{V_b}{I_b}} \quad \frac{i_{ds}}{I_b} - \frac{\omega L_{ss}}{\frac{V_b}{I_b}} \quad \frac{i_{qs}}{I_b} - \frac{\omega L_M}{\frac{V_b}{I_b}} \frac{p}{\omega} \frac{i_{dr}}{I_b}$$

$$+ \frac{\omega L_M}{\frac{V_b}{I_b}} \quad \frac{i_{qr}}{I_B}$$

$$V_{sm}(p.u) = \frac{R_{ss}+X_{ss}\frac{p}{\omega}}{Z_b} \cdot \frac{i_{ds}}{I_b} - \frac{X_{ss}}{Z_b} \cdot \frac{i_{qs}}{I_b} - \frac{X_M}{Z_b} \frac{p}{\omega} \frac{i_{dr}}{I_b}$$

$$+ \frac{X_M}{Z_b} \frac{i_{qr}}{I_b}$$

$$V_{sm}(p.u) = [R_{ss}(p.u.) + X_{ss}(p.u.) \frac{p}{\omega}] \, i_{ds}(p.u.) - X_{ss}(p.u.) \, i_{ds}(p.u$$

$$-X_M(p.u.) \cdot \frac{p}{\omega} \cdot i_{dr}(p.u.) + X_M(p.u.) \, i_{qr}(p.u.)$$

$$\ldots(2.38)$$

Remaining stator and rotor voltage equations can be converted into the per-unit form in a similar way. Now the suffix p.u. from all the quantities is dropped for simplicity. Final voltage current equation for the system can be expressed as

$$
\begin{bmatrix}
V_{sm} \\
0 \\
aa_T V_{sm} \cos(\pi-\alpha)\cos\alpha_r \\
aa_T V_{sm} \cos(\pi-\alpha)\sin\alpha_r
\end{bmatrix}
=
\begin{bmatrix}
(R_{ss}+X_{ss}\frac{p}{\omega}) & -X_{ss} & X_M\frac{p}{\omega} & -X_M \\
X_{ss} & (R_{ss}+X_{ss}\frac{p}{\omega}) & X_M & X_M\frac{p}{\omega} \\
X_M\frac{p}{\omega} & -sX_M & (R_{eq}+X_{eq}\frac{p}{\omega}) & -sX_{rr} \\
sX_M & X_M\frac{p}{\omega} & sX_{rr} & (R_{eq}+X
\end{bmatrix}
$$

$$
X
\begin{bmatrix}
i_{ds} \\
i_{qs} \\
-i_{rm}\cos\alpha_r \\
-i_{rm}\sin\alpha_r
\end{bmatrix}
\quad \ldots(2.39)
$$

Electromagnetic torque equation (2.37) for the system can also be converted to per unit form by dividing with $T_{base}$.

$$\frac{T_e}{T_b} = \frac{\frac{3}{2}\frac{P}{2} L_M (i_{ds}\,i_{qr} - i_{qs}\,i_{dr})}{T_b}$$

$$T_e(p.u) = \frac{\frac{3}{2}\frac{P}{2} L_M (i_{ds}\,i_{qr} - i_{qs}\,i_{dr})}{\frac{3}{2} V_b\,i_b\,/\,\omega_b}$$

$$= \frac{\frac{P}{2} L_M \frac{2}{P} \omega}{Z_b} \left[ \frac{i_{ds}}{I_b} \frac{i_{qr}}{I_b} - \frac{i_{qs}}{I_b} \frac{i_{dr}}{I_b} \right]$$

$$= \frac{X_M}{Z_b} \left[ i_{ds}(p.u.) \, i_{qr}(p.u.) - i_{qs}(p.u.) \, i_{dr}(p.u.) \right]$$

$$T_e(p.u.) = X_M(p.u.) \left[ i_{ds}(p.u.) \, i_{qr}(p.u.) - i_{qs}(p.u.) \, i_{dr}(p.u.) \right]$$

dropping the suffix p.u. in above equation

$$T_e = X_M \left( i_{ds} \, i_{qr} - i_{qs} \, i_{dr} \right) \qquad \qquad ...(2.40)$$

Equations (2.39) and equation (2.40) in per unit form completely describe the behaviour of the drive.

## 2.4 CONCLUSIONS

The idealized model developed on the concept of coupled circuit approach is well suited for determining the dominant features of this system. The assumptions made in developing the model are quite justified for most of practical purposes. The model is simple for carrying out steady state and dynamic analysis.

# CHAPTER - III

## STEADY STATE ANALYSIS

### 3.1 INTRODUCTION

This chapter deals with the steady state analysis of slip power recovery drive. Expressions for torque, supply current, power factor, efficiency and d.c.link current are derived using the mathematical model developed in chapter II. Steady state performance has been investigated at different firing angles.

### 3.2 EQUATIONS OF THE DRIVE UNDER STEADY STATE

During steady state, the different phase voltages and phase currents attain a steady state value and appear d.c. in nature, when refferred to a d-q axes synchronously rotating reference frame. Hence their time derivatives would fall to zero. Thus steady state equations of the system are obtained from the equations (2.39) by replacing all the terms associated with p by zeros. Hence final steady state equations can be expressed as

$$
\begin{bmatrix}
V_{sm} \\
0 \\
aa_T V_{sm} \cos(\pi-\alpha)\cos \alpha_{ro} \\
aa_T V_{sm} \cos(\pi-\alpha)\sin \alpha_{ro}
\end{bmatrix}
=
\begin{bmatrix}
R_{ss} & -X_{ss} & 0 & -X_M \\
X_{ss} & R_{ss} & X_M & 0 \\
0 & -s_o X_M & R_{eq} & -s_o X_{rr} \\
s_o X_M & 0 & s_o X_{rr} & R_{eq}
\end{bmatrix}
\cdot
\begin{bmatrix}
i_{dso} \\
i_{qso} \\
-i_{rmo}\cos \alpha_r \\
-i_{rmo}\sin \alpha_r
\end{bmatrix}
$$

$$...(3.1)$$

Where steady state quantities are identified by subscript 'o.'

For given values of $s_o, \alpha$ and $V_{sm}$ above equations may be simultaneously solved to calculate the values of $i_{dso}, i_{qso}, i_{rmo}$ and $\alpha_{ro}$. Substituting these values in equations (2.21) values of $i_{dro}$ and $i_{qro}$ can be obtained. Torque developed by the drive may be calculated using equation (2.40).

### 3.2.1 Solution of Steady State Equations

Equations (3.1) can be solved by combining first two and last two equations togather, as shown below.

$$V_{sm} + j \cdot o = R_{ss}i_{dso} - X_{ss} i_{qso} + X_M i_{rmo} \sin \alpha_{ro}$$

$$+ j[X_{ss} i_{dso} + R_{ss} i_{qso} - X_m i_{rmo} \cos \alpha_{ro}]$$

$$V_{sm} \angle 0 = R_{ss}(i_{dso} + j i_{qso}) + j X_{ss}(i_{dso} + j i_{qso})$$

$$- j X_M i_{rmo} [\cos \alpha_{ro} + j \sin \alpha_{ro}]$$

$$V_{sm} \angle 0 = (R_{ss} + j X_{ss}) \hat{i}_{smo} - j X_m i_{rmo} \angle \alpha_{ro}$$

$$\ldots (3.2)$$

Where $i_{smo}$ is the peak value of stator phase current under steady state.

Similarly combining last two equations of equations (3.1)

$$aa_T\, V_{sm}\, \cos(\pi-\alpha)\,[\cos \alpha_{ro} + j \sin \alpha_{ro}]$$

$$= -s_o X_M\, i_{qso} - R_{eq}\, i_{rmo}\, \cos \alpha_{ro} + s_o X_{rr}\, i_{rmo}\, \sin \alpha_{ro}$$

$$+j\,[s_o X_M\, i_{dso} - s_o X_{rr}\, i_{rmo}\, \cos \alpha_{ro} - R_{eq}\, i_{rmo} \sin \alpha_r$$

$$aa_T V_{sm}\, \cos(\pi-\alpha)\, \angle\alpha_{ro} = j\, s_o X_M[i_{dso} + j\, i_{qso}] - R_{eq}\, i_{rmo}\, X$$

$$[\cos \alpha_{ro} + j \sin \alpha_{ro}] - j\, s_o X_{rr}\, i_{rmo}[\cos \alpha_{ro} + j\sin \alpha_{ro}$$

so,

$$aa_T V_{sm}\, \cos(\pi-\alpha)\angle\alpha_{ro} + R_{eq}\, i_{rmo}\, \angle\alpha_{ro} + j\, s_o X_{rr}\, i_{rmo}\angle\alpha_{ro} = j\, s_o X_M\, \hat{i}$$

or

$$\hat{i}_{smo} = \frac{[aa_T V_{sm}\, \cos(\pi-\alpha) + R_{eq}\, i_{rmo} + j\, s_o X_{rr}\, i_{rmo}]\, \angle\alpha_{ro}}{j\, s_o X_M}$$

$$\dots(3.3)$$

Substituting equation (3.3) in equation (3.2)

$$V_{sm} \angle 0 = (R_{ss} + j\, X_{ss})\, \frac{[aa_T V_{sm}\, \cos(\pi-\alpha) + R_{eq}\, i_{rmo} + j\, s_o X_{rr} i_{rmo}]\angle}{j\, s_o X_M}$$

$$- j\, X_M\, i_{rmo} \angle\, \alpha_{ro}$$

$$\frac{j\, s_o X_M V_{sm} \angle-\alpha_{ro}}{(R_{ss} + j\, X_{ss})} = aa_T V_{sm}\, \cos(\pi-\alpha) + R_{eq}\, i_{rmo} + j\, s_o X_{rr}\, i_{rmo}$$

$$+ \frac{X_M^2\, s_o\, i_{rmo}}{(R_{ss} + j X_{ss})}$$

$$\frac{s_o X_M\, V_{sm} \angle \frac{\pi}{2} - \alpha_{ro} - \tan^{-1}\frac{X_{ss}}{R_{ss}}}{\sqrt{R_{ss}^2 + X_{ss}^2}} = aa_T V_{sm}\, \cos(\pi-\alpha) + R_{eq}\, i_{rmo}$$

$$+ j\, s_o X_{rr}\, i_{rmo} + \frac{X_M^2\, s_o\, i_{rmo}}{R_{ss}^2 + X_{ss}^2}(R_{ss}$$

$$- j X_s$$

$$\frac{s_o X_M V_{sm} \left/ \dfrac{\pi}{2} - \alpha_{ro} - \tan^{-1} \dfrac{X_{ss}}{R_{ss}} \right.}{\sqrt{R_{ss}^2 + X_{ss}^2}} = aa_T V_{sm} \cos(\pi - \alpha)$$

$$+ \left[ \left( R_{eq} + \frac{s_o X_M^2 R_{ss}}{R_{ss}^2 + X_{ss}^2} \right) + j \left( s_o X_{rr} - \frac{s_o X_{ss} X_M^2}{R_{ss}^2 + X_{ss}^2} \right) \right] i_{rmo}$$

or

$$Z_1 \left/ \frac{\pi}{2} - \alpha_{ro} - \tan^{-1} \frac{X_{ss}}{R_{ss}} \right. = Z_2 + (Z_3 + iZ_4) \, i_{rmo}$$

$$\ldots (3.4)$$

where

$$Z_1 = \frac{s_o X_M V_{sm}}{\sqrt{R_{ss}^2 + X_{ss}^2}}$$

$$Z_2 = aa_T V_{sm} \cos(\pi - \alpha)$$

$$Z_3 = R_{eq} + \frac{s_o X_M^2 R_{ss}}{R_{ss}^2 + X_{ss}^2}$$

$$Z_4 = s_o X_{rr} - \frac{s_o X_{ss} X_M^2}{R_{ss}^2 + X_{ss}^2}$$

Equating the magnitudes on both sides in equation (3.4)

$$Z_1^2 = (Z_2 + Z_3 \, i_{rmo})^2 + (Z_4 \, i_{rmo})^2$$

or

$$Z_1^2 = Z_2^2 + 2Z_2 Z_3 \, i_{rmo} + (Z_3^2 + Z_4^2) \, i_{rmo}^2$$

or

$$i_{rmo}^2 [z_3^2 + z_4^2] + 2z_2 z_3 i_{rmo} + z_2^2 - z_1^2 = 0$$

or

$$z_5 i_{rmo}^2 + z_6 i_{rmo} + z_7 = 0 \qquad \qquad \ldots(3.5)$$

where,

$$z_5 = z_3^2 + z_4^2$$

$$z_6 = 2z_2 z_3$$
$$z_7 = z_2^2 - z_1^2$$

Equation (3.5) is a quadratic equation in $i_{rmo}$ which can be solved to obtain two values for $i_{rmo}$. The positive value gives the magnitude of $i_{rmo}$.

$$i_{rmo} = \frac{-z_6 + \sqrt{z_6^2 - 4z_5 z_7}}{2z_5} \qquad \qquad \ldots(3.6)$$

Similarly equating the angle on both sides of equation (3.4)

$$\frac{\pi}{2} - \alpha_{ro} - \tan^{-1} \frac{X_{ss}}{R_{ss}} = \tan^{-1} \frac{z_4 i_{rmo}}{z_2 + z_3 i_{rmo}}$$

or

$$\alpha_{ro} = \frac{\pi}{2} - \tan^{-1} \frac{X_{ss}}{R_{ss}} - \tan^{-1} \frac{z_4 i_{rmo}}{z_2 + z_3 i_{rmo}}$$

$$\ldots(3.7)$$

Having determined $\alpha_{ro}$ and $i_{rmo}$, the phasor $\hat{i}_{smo}$ can be determined from equation (3.3). The value of $i_{dso}$ and $i_{qso}$ can be determined from phasor $\hat{i}_{smo}$ as real and imaginary parts respectively. After determining $\alpha_{ro}$, $i_{rmo}$, $i_{dso}$ and $i_{qso}$, the complete performance of the drive can be determined as given below.

## 3.2.2 Equation of No Load Slip

Under ideal no load condition, the torque developed by the drive is zero i.e. rotor current is zero. The no load slip $s_{nl}$ of the drive is calculated by putting rotor current to be zero in equation (2.22).

$$V_R = V_I + (R_F + L_F p)\, i_R$$

if $i_R = 0$, $V_R = V_I$

Substituting for $V_R$ and $V_I$ from equation (2.13) and equation (2.23),

$$\frac{3\sqrt{3}}{\pi} V_{rm} = \frac{3\sqrt{3}}{\pi} a_T V_{sm} \cos(\pi - \alpha)$$

$$s_{nl} \frac{V_{sm}}{a} = a_T V_{sm} \cos(\pi - \alpha)$$

$$s_{nl} = a \cdot a_T \cos(\pi - \alpha) \qquad \qquad \ldots(3.8)$$

## 3.2.3 Expressions of Stator Current

If phase currents are lagging the phase voltages by $\phi^\circ$, then refferring to equations(2.8), expression for phase currents may be written as

$$i_{aso} = i_{smo} \cos(\theta - \phi)$$

$$i_{bso} = i_{smo} \cos\left(\theta - \phi - \frac{2\pi}{3}\right)$$

$$i_{cso} = i_{smo} \cos\left(\theta - \phi + \frac{2\pi}{3}\right) \qquad \ldots(3.9)$$

Resolving these along d axis, $i_{dso}$ may be written as

$$i_{dso} = \frac{2}{3} [ \, i_{aso} \cos \theta + i_{bso} \cos (\theta - \frac{2\pi}{3}) + i_{cso} \cos(\theta + \frac{2\pi}{3}) ]$$

$$...(3.10)$$

Substituting equations (3.9) in equation (3.10) and sim-plifying

$$i_{dso} = i_{smo} \cos \phi \qquad\qquad ...(3.11)$$

Similarly

$$i_{qso} = -i_{smo} \sin \phi \qquad\qquad ...(3.12)$$

Combining equation (3.11) and equation (3.12)

$$i_{smo} = \sqrt{i_{dso}^2 + i_{qso}^2} \qquad\qquad ...(3.13)$$

or

$$I_s = \frac{1}{\sqrt{2}} \sqrt{i_{dso}^2 + i_{qso}^2} \qquad\qquad ...(3.14)$$

where $I_s$ is the r.m.s value of stator phase current.

### 3.2.4 Expression For Supply Current and Power Factor

In slip power recovery scheme, the output current of the inverter is fed back to the supply, hence the net current drawn from the supply is the phasor difference of the stator current and the inverter current fed back to the supply. If $i_{dIo}$ and $i_{qIo}$ are the direct and quadrature component of the inverter feedback current respectively, the net feedback current is given by

$$\hat{i}_{fbo} = i_{dIo} + j\, i_{qIo} \qquad \qquad \ldots (3.15)$$

Assuming no harmonics in the inverter feed back current and no losses in the inverter, the power balance equation for inverter may be written as

Power on d.c side of inverter = Power on a.c.side
of inverter

or

$$V_I \cdot i_{Ro} = \frac{3}{2}\, (a_T V_{dso} \cdot i_{dIo} + a_T V_{qso} \cdot i_{qIo}) \ldots (3.16)$$

Since the angular relationship between d axis and the magnetic axes of stator and rotor phases is so chosen that these coincide at time $t = 0$, hence

$$V_{dso} = V_{sm} \quad \text{and } V_{qso} = 0$$

Substituting above values in equation (3.16) and substituting for $V_I$ from equation (2.23) in equation (3.16).

$$\frac{3\sqrt{3}}{\pi}\, a_T\, V_{sm}\, \cos\,(\pi - \alpha) \cdot i_{Ro} = \frac{3}{2}\, a_T\, V_{sm}\, i_{dIo}$$

or

$$i_{dIo} = \frac{2\sqrt{3}}{\pi}\, i_{Ro}\, \cos\,(\pi - \alpha) \qquad \ldots (3.17)$$

Substituting $i_{RO}$ from equation (2.14) in equation (3.17)

$$i_{dIo} = i_{rmo}\, \cos\,(\pi - \alpha) \qquad \ldots (3.18)$$

As all the computations are made with quantities referred to stator, referring equation (3.18) to stator

$$i'_{dIo} = i'_{rmo} \cos (\pi - \alpha) \qquad \qquad ...(3.19)$$

As in the computation, referred quantities are used without prime, droping the prime from equation (3.19)

$$i_{dIo} = i_{rmo} \cos (\pi - \alpha) \qquad \qquad ...(3.20)$$

Since the fundamental component of the inverter feed back current lagsby firing angle $\alpha$ with the voltage on a.c. side of inverter, we.can write

$$\frac{i_{dIo}}{i_{qIo}} = \frac{I_{fbo} \cos (-\alpha)}{I_{fbo} \sin (-\alpha)}$$

or

$$i_{qIo} = -\ i_{dIo} \tan \alpha \qquad \qquad ...(3.21)$$

Substituting from equation (3.21) in equation (3.15), the inverter fed back current is given by

$$\hat{i}_{fbo} = i_{dIo} - j\ i_{dIo} \tan \alpha \qquad \qquad ...(3.22)$$

Since the supply current is the phasor difference of stator current and inverter feed back current, so

Supply current

$$\hat{i}_L = \hat{i}_{smo} - \hat{i}_{fbo} \qquad \qquad ...(3.23)$$

Substituting from equation (3.22) in equation (3.23)

$$\hat{i}_L = (i_{dso} + j\ i_{qso}) - (i_{dIo} - j\ i_{dIo}\ \tan \alpha)$$

or

$$\hat{i}_L = (i_{dso} - i_{dIo}) + j\ (i_{qso} + i_{dIo}\ \tan \alpha)$$

or

Supply current

$$|I_L| = \sqrt{(i_{dso} - i_{dIo})^2 + (i_{qso} + i_{dIo}\ \tan \alpha)^2}$$

$$\ldots (3.24)$$

and r.m.s value of supply current

$$|I_L|_{rms} = \frac{|I_L|}{\sqrt{2}} \qquad \ldots (3.25)$$

The power factor is obtained as

$$\cos \phi_L = \frac{(i_{dso} - i_{dIo})}{|I_L|} \qquad \ldots (3.26)$$

3.2.5 Expression for D.C.Link Current

Combining equations (2.21)

$$i_{rmo} = \sqrt{i_{dro}^2 + i_{qro}^2}$$

Substituting above equation in equation (2.14)

$$i_R = \frac{\pi}{2\sqrt{3}} \sqrt{i_{dro}^2 + i_{qro}^2} \qquad \ldots (3.27)$$

3.2.6 Expression for Power Input, Power Output and
Efficiency

Net power input to the drive

$$P_I = 3 \ (V_{ph})_{rms} \cdot \text{supply current}_{rms} \cdot \cos \phi_L$$

$$= 3 \ \frac{V_{sm}}{\sqrt{2}} \cdot \frac{|I_L|}{\sqrt{2}} \cdot \cos \phi_L$$

$$= \frac{3}{2} \ V_{sm} \cdot |I_L| \cdot \cos \phi_L \qquad \qquad \ldots (3.28)$$

Air gap power $P_{ag} = T_{eo}$ $\qquad \qquad \ldots (3.29)$

Mechanical power developed including friction and windage losses

$$P_m = (1 - s_o) \ T_{eo} \qquad \qquad \ldots (3.30)$$

Neglecting friction and windage losses

Output power $\qquad P_o = P_m$

or

$$P_o = (1 - s_o) \ T_{eo} \qquad \qquad \ldots (3.31)$$

Hence efficiency of the drive

$$= \frac{P_o}{P_I} \times 100 \ \% \qquad \qquad \ldots (3.32)$$

## 3.3 ANALYTICAL RESULTS AND DISCUSSIONS

Steady state performance of the drive has been computed by simulating the steady state equations on a digital computer. Flowchart for digital simulation is presented in Appendix- III. The computer programme has been developed in FORTRAN language. The measured parameters of the drive are given in Appendix- II.

3.3.1 Variation of No Load Slip

The no load slip is computed using equation (3.3).
Variation of no load slip $s_{nl}$ with firing angle is
shown in Fig. 3.1. By controlling firing angle of the
inverter, wide range speed control can be obtained in
subsynchronous motoring operation.

3.3.2 Torque-Slip Characteristics

Electromagnetic torque developed by the drive is
computed by equation (2.40). The torque vs slip charac-
teristics at different fixing angle settings are shown in
Fig. 3.2. It is observed that the torque-slip characteris-
tic is almost linear for a given value of firing angle. It
is also evident that the starting torque falls with increase
in firing angle. Fig. 3.2 shows that the system behaves as
a fairly good variable speed drive in subsynchronous motoring
operation with inverter firing angle in the recovery loop as
a speed control parameter.

3.3.3 Torque-Supply Current Characteristics

Supply current drawn by the drive has been computed
using equation (3.25). Fig. 3.3 depicts the torque vs supply
current for different settings of firing angle. The torque -
supply current characteristics of the drive are similar to
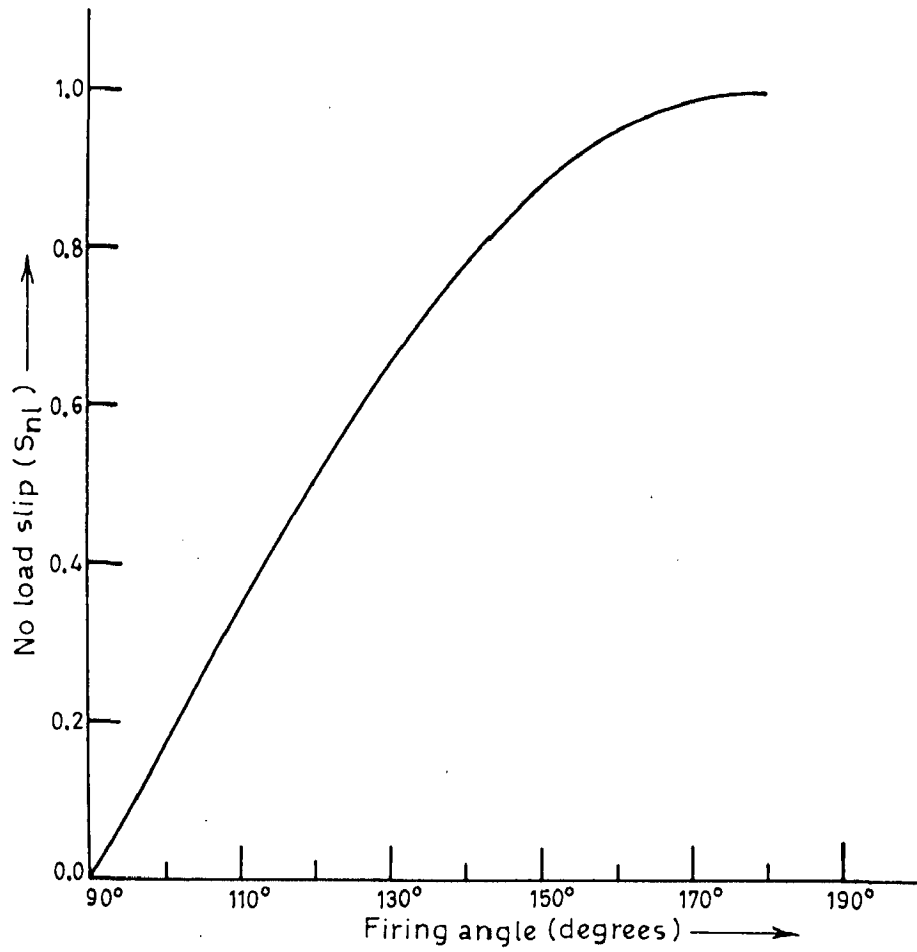that of a separately excited d.c. motor.

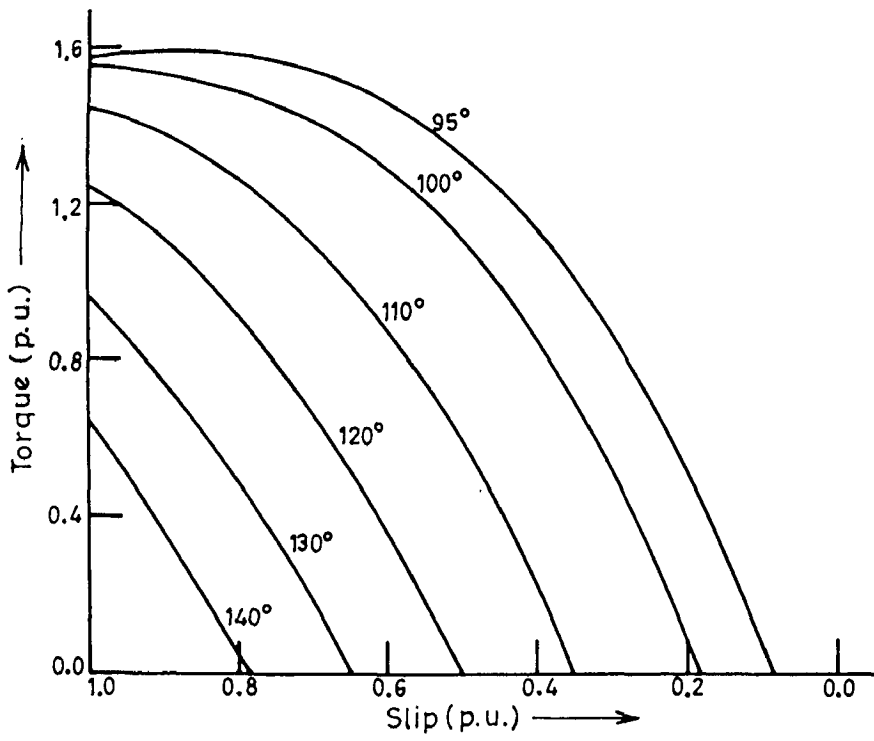Fig.3.1: Variation of no load slip with firing angle.

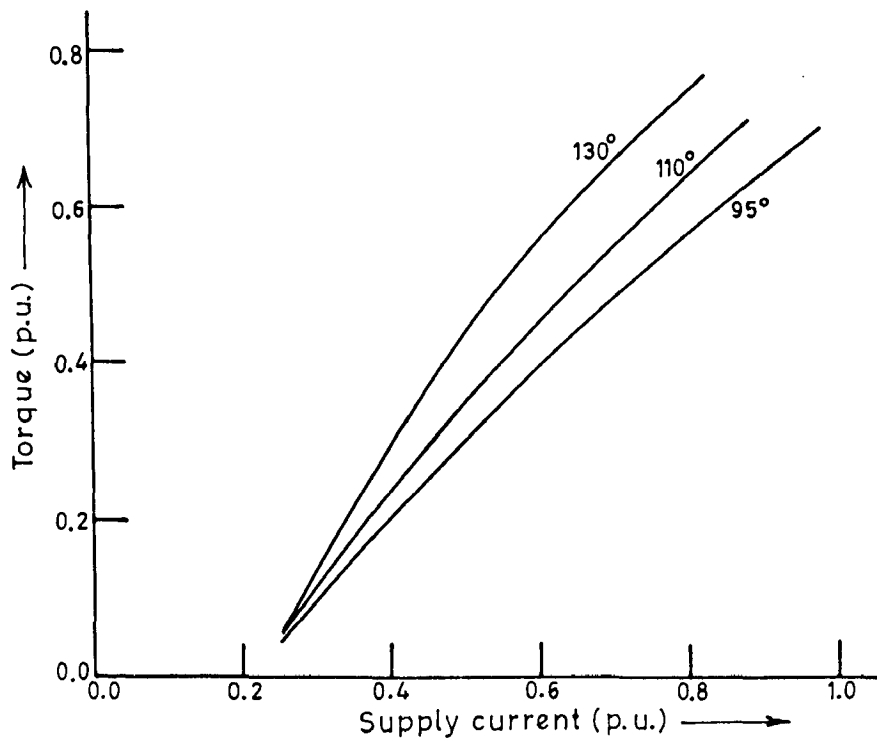Fig. 3.2: Torque - slip characteristics at different settings of firing angle.



Fig. 3.3: Torque - supply current characteristics.

3.3.4 Power Factor-Slip Characteristics

Overall power factor of the drive has been computed using equation (3.26). Fig 3.4 shows the power factor-slip characteristics at different settings of firing angle. It is evident that the power factor of the drive is poor for all the values of slip.Power factor further reduces with increasing firing angle. At low values of firing angle, the inverter draws more reactive power and hence reduces the power factor. At higher values of firing angle although, inverter draws less reactive power, but induction motor - rectifier unit operates at low power factor and reduces the overall power factor of the drive.

3.3.5 Efficiency-Slip Characteristics

The efficiency of the drive has been computed using equation (3.32). The variation of efficiency with slip for different firing angles of the inverter is plotted in Fig. 3.5. Compared to conventional induction motor, the efficiency of the drive is much more improved. The improvement in the efficiency is more at lower speed of operation. This is because of larger amount of power recovered at lower speeds of operation.

3.3.6 Supply Current- Slip Characteristics

Fig. 3.6 shows the supply current vs slip characteristics for different values of firing angle. The curves show
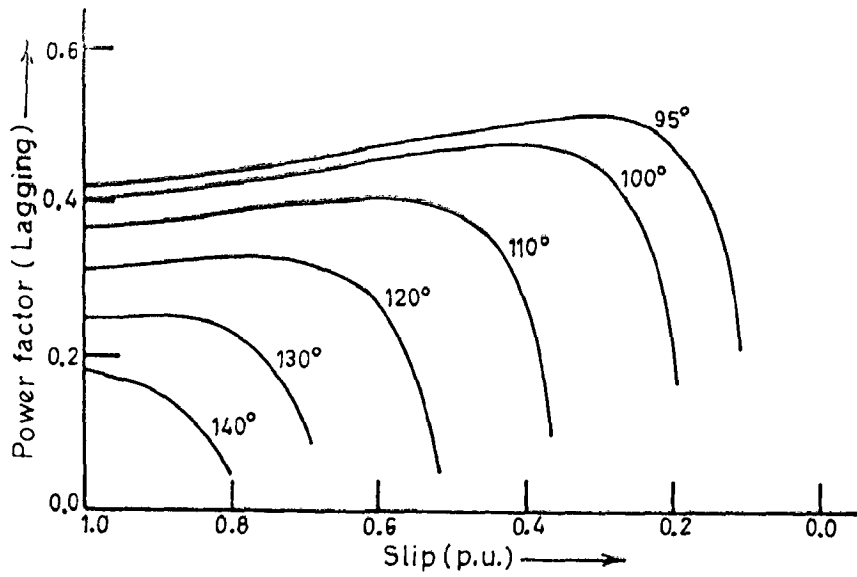
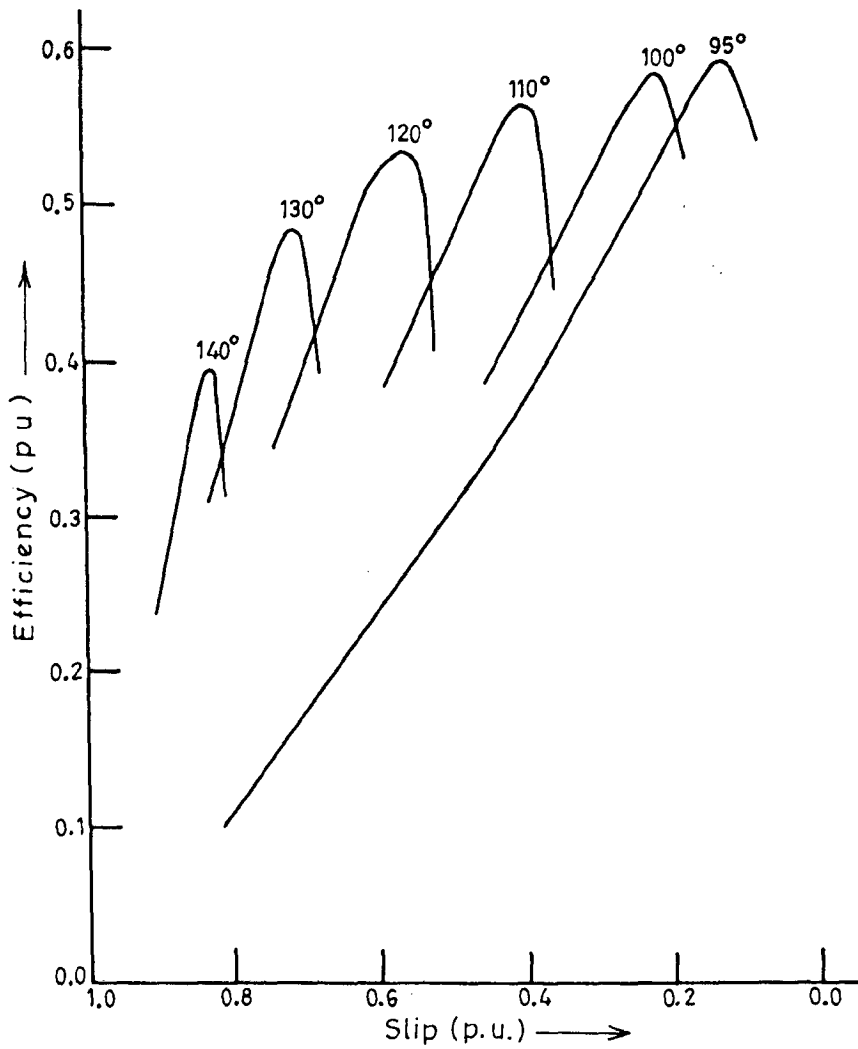Fig.3.4: Power factor - slip characteristics at
different firing angles.



Fig.3.5: Efficiency - slip characteristics at
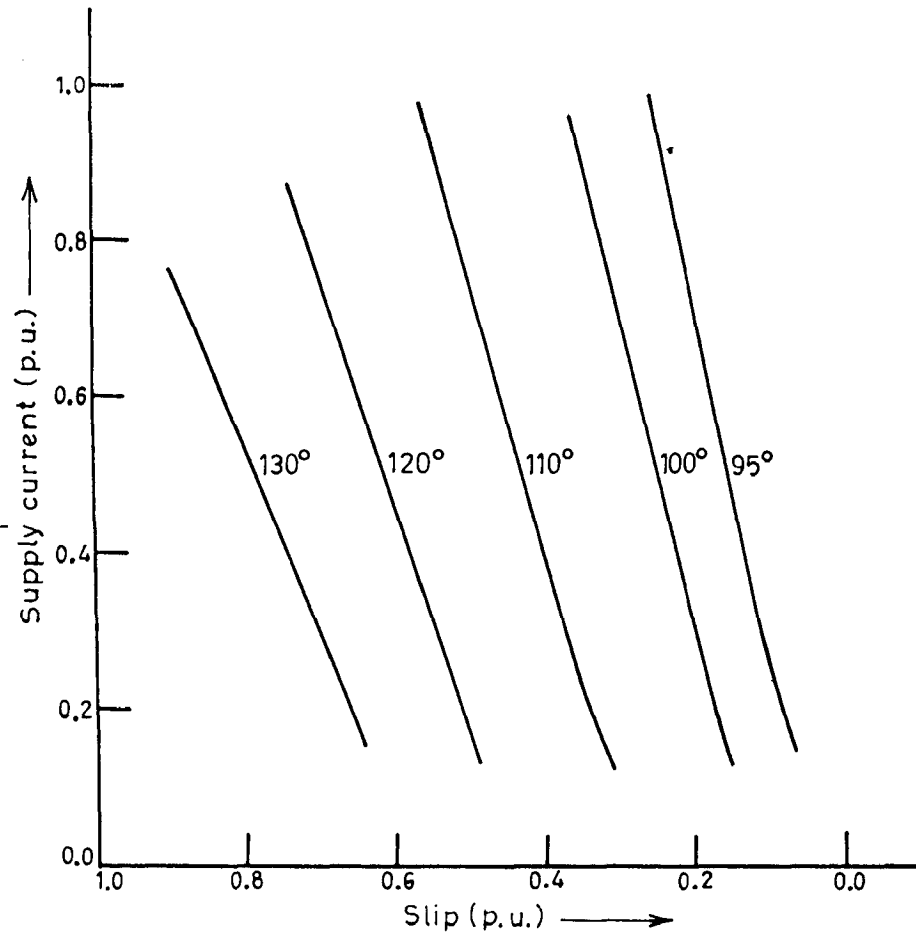different firing angles.

Fig.3.6: Supply current - slip characteristics at different firing angles.
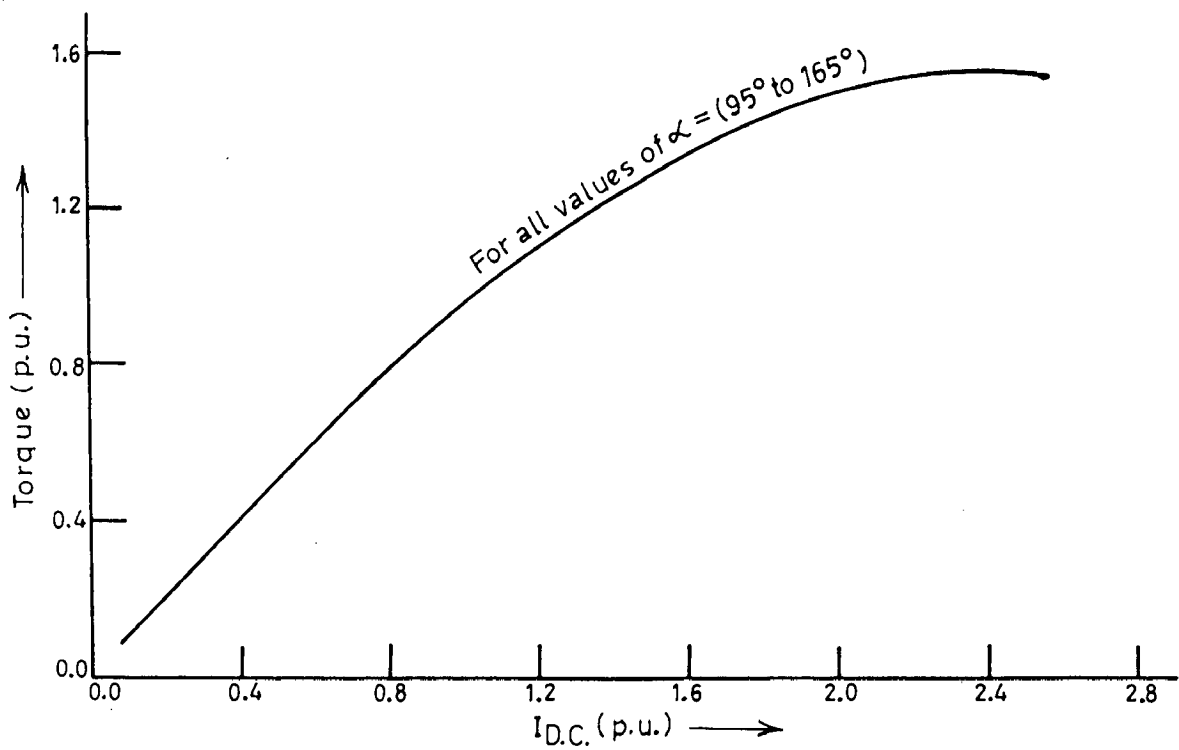
Fig.3.7 : Torque - d.c.link current characteristics.

that the supply current increases with the slip for operation at a fixed firing angle of the inverter.

3.3.7 Relationship Between Developed Torque and D.C. Link Current.

The curve for d.c. link current with developed torque is shown in Fig. 3.7. The curve shows that the developed torque is almost directly proportional to d.c. link current and is independent of firing angle of the inverter.

3.4 CONCLUSIONS

The expressions have been developed to predetermine the performance of the slip power recovery scheme in terms of parameters measured at the terminals of the machine. The drive equations developed are simple and useful for predicting the operating characteristics of the drive. It is observed that the slip power recovery drive exhibits the characteristics similar to that of a separately exited d.c. motor. The full range of speed control can be achieved with inverter firing angle as control parameter.

# CHAPTER - IV

## DESIGN AND DEVELOPMENT OF MICROPROCESSOR
## CONTROLLED LINE COMMUTATED INVERTER

### 4.1 INTRODUCTION

The dramatic advances in semiconductor technology have made available smaller, faster microprocessors at low cost. It has found increasing industrial applications owing to its reliability, flexibility and decreasing cost. In process control industries, it is necessary to adjust the motor speed over a wide range with good speed resolution and reproducibility, with fewer components, these requirements can be easily and cheaply met with microprocessor. Better speed accuracy can be obtained with mic - roprocessor based closed loop control of the drive. The analog firing control schemes have several disadvantages such as difficulty in accurately transmitting analog signal, nonlinearity in the analog transducers, errors due to temperature, component aging, drift and offset of analog components, extraneous disturbances, in flexibility etc.

A digital control scheme is free from these disad - vantages. A microprocessor based control scheme for motor drives promisses several distinct advantages such as fle- xibility, improved performance and economic viability. Most important among these is flexibility. The control

scheme is implemented through software. Therefore to change the control scheme in order to obtain a different drive characteristics or add a new control function, only the software needs to be modified, with minimal or no change in the hardware. Microprocessor based drives can have built in fault finding programs, with a view to take corrective action quickly and effectively.

4.2 PHILOSOPHY OF MICROPROCESSOR BASED FIRING SCHEME

The block diagram of the scheme used for generating the firing pulses is as shown in Fig. 4.1 [23]. It consists of three single phase power isolation signal transformer with Delta-Star connection, zerocrossing detector circuit, pulse amplifier circuit and microprocessor kit consisting of 8085up, memory and PPIs among others [ 29 - 31]. The software must be capable of performing the following tasks sequentially after every 1/6 th period of supply frequency, when executed: -

(i)     Compute the slot of the given firing angle, i.e. if the firing angle lies between 0-60$^o$ or 60$^o$ to 120$^o$ or 120$^o$ to 180$^o$.

(ii)    Adjust the firing angle between 0-60$^o$ and modify the firing command pointer.

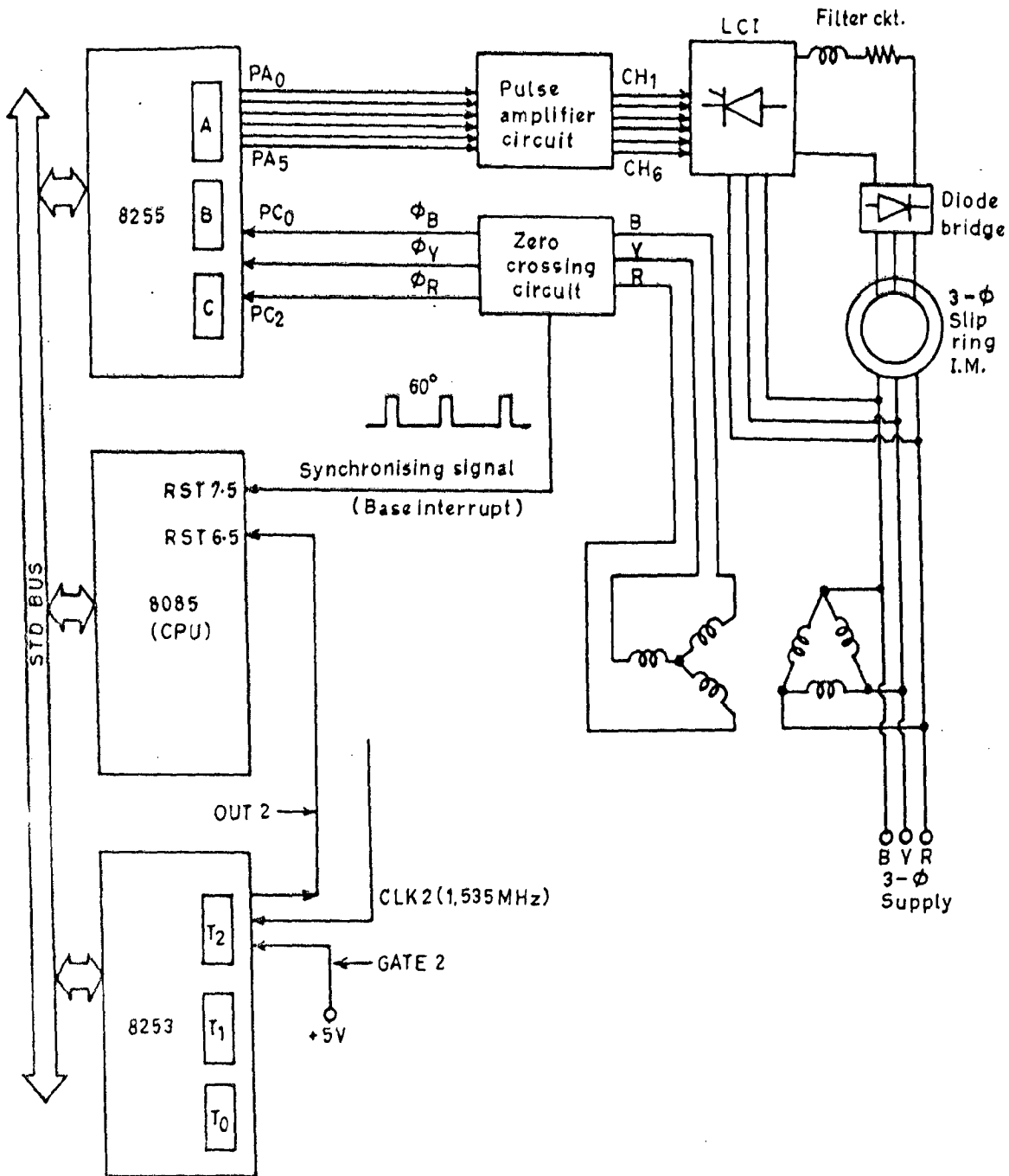(iii)   Proportional to modified firing angle, load a delay word in counter 2 of 8253 timer from delay word table.

Fig.4.1: Block diagram of LCI firing angle control scheme.

(iv)    Check the status of three digital signals
        $\phi_R$, $\phi_Y$ and $\phi_B$. These signals are in phase
        with line voltages $V_{RY}$, $V_{YB}$ and $V_{BR}$ respec-
        tively .

(v)     Depending upon the status of $\phi_R$, $\phi_Y$ and $\phi_B$,
        a firing command word is selected from the
        firing command table.

(vi)    Two SCR's, as selected by high bits of firing
        command word, are fired.

Independently of the algorithm used to control thy-
ristors firing of line commutated inverter, the signals that
synchronises them with the alternating supply voltages are
very necessary. The six SCR bridge inverter circuit will
require six such signals in one cycle of input supply. These
signals are the zerocrossing signals of the line voltages.
These are used by microprocessor to program a delay proportional
to firing angle. The zero crossing circuit gives a train of
pulses as shown in Fig. 4.2 displaced by $60^o$. This train of
pulses is used as base interrupt signals to interrupt micro-
processor after every $60^o$ interval via RST 7.5 interrupt.
Three digital power signals are obtained from zero crossing
detector circuit. These signals $\phi_R$, $\phi_Y$ and $\phi_B$ are in phase
with supply line voltages $V_{RY}$, $V_{YB}$ and $V_{BR}$ respectively. The
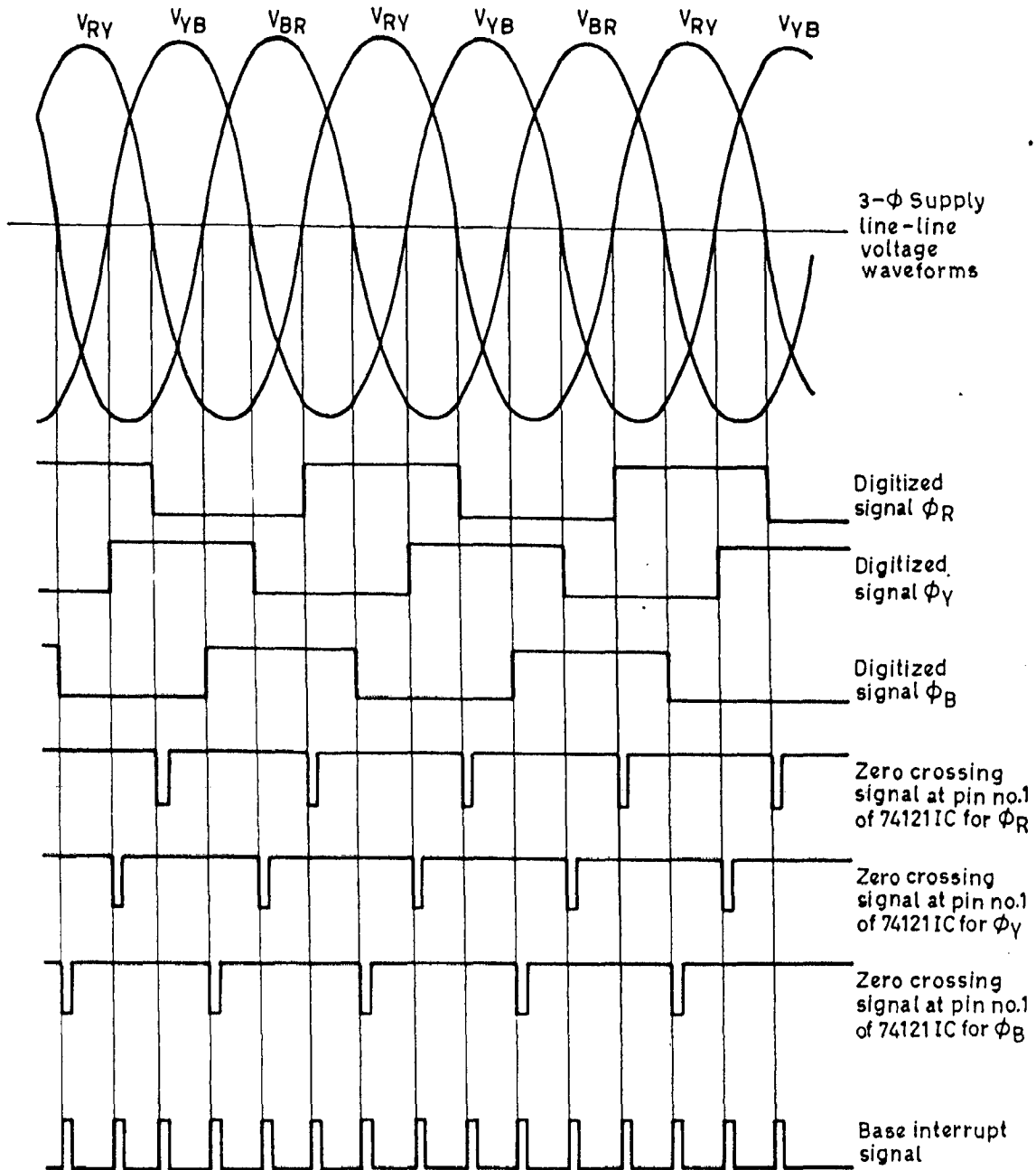status of these signals is read by microprocessor in every

Fig. 4.2: Theoretical waveforms for base interrupt
generation circuit (refer to fig. 4.4).

$60^{\circ}$ interval through Port -C of PPI 8255. These signals have six distinct values for each $60^{\circ}$ interval. The thyristor pair to be triggered in a particular $60^{\circ}$ interval depends upon the status of signals $\phi_R$, $\phi_Y$ and $\phi_B$ and slot of firing angle i.e. whether $0-60^{\circ}$, $60-120^{\circ}$, $120^{\circ}-180^{\circ}$. A firing command table [Table 4.1] is prepared for each slot of firing angle i.e. $0-60^{\circ}$, $60^{\circ}-120^2$, $120^{\circ}-180^{\circ}$ based on different status of digitized signals, $\phi_R,\phi_Y,\phi_B$. This firing command data table denotes the numbers of thyristors that are to be fired, for a particular type of digitized power signals those are high, in the specified period as shown in Fig. 4.3. By this algorithm, the full range of $0-180^{\circ}$can be controlled with one sixth period of a.c. source.

Fig. 4.3 gives the relationship between the firing angle range ($0-60^{\circ}$, $60^{\circ}-120^{\circ}$, $120^{\circ}-180^{\circ}$) and the quantized signals $\phi_R,\phi_Y$ and $\phi_B$ in deciding the pair of thyristors to be triggered. For example,if $120 < \alpha < 180$ and quantized signals $\phi_R$, $\phi_Y$ , $\phi_B$ are 101, then thyristors 3 and 4 must be fired. The relevent power circuit is also shown in Fig. 4.3. The firing commands (i.e. pair of thyristors to be turn ON) are outputed via bits $PA_0$ to $PA_5$ of I/O 8255 chip for thyristors $T_1$ to $T_6$. Hence the control word to fire thyristors 3 and 4 will be $PA_7 - PA_0 =$ X X 001100 i.e. 12H. The Table 4.1 shows (0 0)
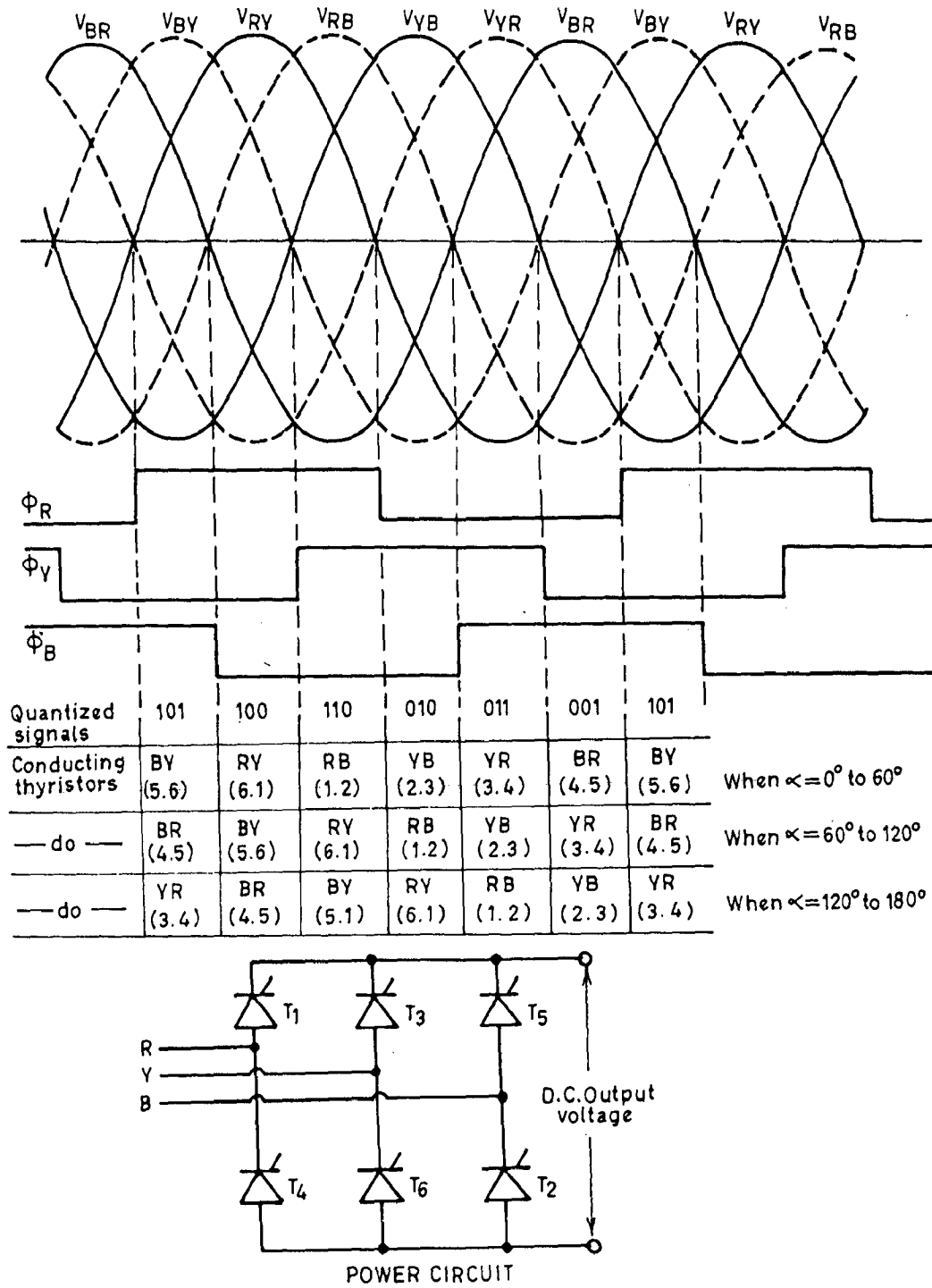
$V_{BR}$  $V_{BY}$  $V_{RY}$  $V_{RB}$  $V_{YB}$  $V_{YR}$  $V_{BR}$  $V_{BY}$  $V_{RY}$  $V_{RB}$

$\Phi_R$

$\Phi_Y$

$\Phi_B$

| Quantized signals | 101 | 100 | 110 | 010 | 011 | 001 | 101 | |
|---|---|---|---|---|---|---|---|---|
| Conducting thyristors | BY (5.6) | RY (6.1) | RB (1.2) | YB (2.3) | YR (3.4) | BR (4.5) | BY (5.6) | When $\alpha = 0°$ to $60°$ |
| —do— | BR (4.5) | BY (5.6) | RY (6.1) | RB (1.2) | YB (2.3) | YR (3.4) | BR (4.5) | When $\alpha = 60°$ to $120°$ |
| —do— | YR (3.4) | BR (4.5) | BY (5.1) | RY (6.1) | RB (1.2) | YB (2.3) | YR (3.4) | When $\alpha = 120°$ to $180°$ |

R
Y
B

$T_1$  $T_3$  $T_5$

$T_4$  $T_6$  $T_2$

D.C. Output voltage

POWER CIRCUIT

Fig. 4.3: Synchronizing signals.

TABLE 4.1

FIRING COMMAND DATA TABLE

Range of firing angle $\alpha = 0°$ to $60°$

| $\phi_R$ | $\phi_Y$ | $\phi_B$ | I quantizer | Address of firing command word | ON SCRs | Firing Command word |
|---|---|---|---|---|---|---|
| 1 | 2 | 3 | 4 | 5 | 6 | 7 |
| 0 | 0 | 1 | 1 | 2100+01 | 4,5 | 00011000 (PA7-PAO) i.e.18H |
| 0 | 1 | 0 | 2 | 2100+02 | 2,3 | 00000110 i.e. 06H |
| 0 | 1 | 1 | 3 | 2100+03 | 3,4 | 00001100 i.e. 0CH |
| 1 | 0 | 0 | 4 | 2100+04 | 6,1 | 00100001 i.e.21H |
| 1 | 0 | 1 | 5 | 2100+05 | 5,6 | 00110000 i.e.30H |
| 1 | 1 | 0 | 6 | 2100+06 | 1,2 | 00000011 i.e.03H |

Range of firing angle $\alpha = 60°$ to $120°$

| 1 | 2 | 3 | 4 | 5 | 6 | 7 |
|---|---|---|---|---|---|---|
| 0 | 0 | 1 | 1 | 2100+07 | 3,4 | 00001100 i.e.0CH |
| 0 | 1 | 0 | 2 | 2100+08 | 1,2 | 00000011 i.e.03H |
| 0 | 1 | 1 | 3 | 2100+09 | 2,3 | 00001100 i.e.06H |
| 1 | 0 | 0 | 4 | 2100+0A | 5,6 | 00110000 i.e.30H |
| 1 | 0 | 1 | 5 | 2100+0B | 4,5 | 00011000 i.e.18H |
| 1 | 1 | 0 | 6 | 2100+0C | 6,1 | 00100001 i.e.21H |

Range of firing angle $\alpha = 120^\circ$ to $180^\circ$

| 1 | 2 | 3 | 4 | 5 | 6 | 7 |
|---|---|---|---|---|---|---|
| 0 | 0 | 1 | 1 | 2100+0D | 2,3 | 00001100 i.e. 06H |
| 0 | 1 | 0 | 2 | 2100+0E | 6,1 | 00100001 i.e. 21H |
| 0 | 1 | 1 | 3 | 2100+0F | 1,2 | 00000011 i.e. 03H |
| 1 | 0 | 0 | 4 | 2100+10 | 4,5 | 00011000 i.e. 18H |
| 1 | 0 | 1 | 5 | 2100+11 | 3,4 | 00001100 i.e. 0CH |
| 1 | 1 | 0 | 6 | 2100+12 | 5,6 | 00110000 i.e.30H |

the control words for different pair of thyristors to be fired.

The digitized signals $\phi_R$, $\phi_Y$ and $\phi_B$ are read via bits PC2, PC1 and PC0 of I/O 8255 chip. In Table 4.1, the digitized signals are arranged in increasing order (001 at lowest address and 110 at the highest address). Thus for a given firing angle range and the digitized signal read, the address of firing command is easily determined.

The microprocessor uses a programmable interval timer chip 8253 to produce the delay required for given value of $\alpha$. The clock frequency input to the timer is 1.535 MHz. The delay word proportional to firing angle $\alpha$ is calculated as follows -

Since $360^\circ$ is equal to 20 m sec.

So $1^\circ$ is equal to $\frac{20}{360}$ m sec.

Period of one clock is $\frac{1}{1.535 \times 10^6}$ secs.

Hence delay word for $1^\circ$ will be

$$\frac{\dfrac{20 \times 10^{-3}}{360}}{\dfrac{1}{1.535 \times 10^6}} = 85_D = 55\ H$$

The delay word is taken to be of 2 byte to accomodate full range from 0 - $60^\circ$, the delay word for $1^\circ$ will be stored as 0055H. Similarly calculations are made for full range 0-60$^\circ$ and are tabulated as given in Table 4.2.

## TABLE 4.2

## DELAY COUNTS

| S.NO. | MEMORY ADDRESS | DELAY COUNT | S.NO. | MEMORY ADDRESS | DELAY COUNT | S.NO. | MEMORY ADDRESS | DELAY COUNT |
|---|---|---|---|---|---|---|---|---|
| 1. | 2200 | 00 | 22. | 2215 | 03 | 43. | 222A | FE |
| 2. | 2201 | 00 | 23. | 2216 | AA | 44. | 222B | 06 |
| 3. | 2202 | 55 | 24. | 2217 | 03 | 45. | 222C | 54 |
| 4. | 2203 | 00 | 25. | 2218 | FF | 46. | 222D | 07 |
| 5. | 2204 | AA | 26. | 2219 | 03 | 47. | 222E | A9 |
| 6. | 2205 | 00 | 27. | 221A | 54 | 48. | 222F | 07 |
| 7. | 2206 | 00 | 28. | 221B | 04 | 49. | 2230 | FE |
| 8. | 2207 | 01 | 29. | 221C | AA | 50. | 2231 | 07 |
| 9. | 2208 | 55 | 30. | 221D | 04 | 51. | 2232 | 53 |
| 10. | 2209 | 01 | 31. | 221E | FF | 52. | 2233 | 08 |
| 11. | 220A | AA | 32. | 221F | 04 | 53. | 2234 | A9 |
| 12. | 220B | 01 | 33. | 2220 | 54 | 54. | 2235 | 08 |
| 13. | 220C | 00 | 34. | 2221 | 05 | 55. | 2236 | FE |
| 14. | 220D | 02 | 35. | 2222 | A9 | 56. | 2237 | 08 |
| 15. | 220E | 54 | 36. | 2223 | 05 | 57. | 2238 | 53 |
| 16. | 220F | 02 | 37. | 2224 | FF | 58. | 2239 | 09 |
| 17. | 2210 | AA | 38. | 2225 | 05 | 59. | 223A | A9 |
| 18. | 2211 | 02 | 39. | 2226 | 54 | 60. | 223B | 09 |
| 19. | 2212 | 00 | 40. | 2227 | 06 | 61. | 223C | FE |
| 20. | 2213 | 03 | 41. | 2228 | A9 | 62. | 223D | 09 |
| 21. | 2214 | 53 | 42. | 2229 | 06 | 63. | 223E | 54 |

TABLE 4.2    contd..

| S.NO. | MEMORY ADDRESS | DELAY COUNT | S.NO. | MEMORY ADDRESS | DELAY COUNT | S.NO. | MEMORY ADDRESS | DELAY COUNT |
|---|---|---|---|---|---|---|---|---|
| 64. | 223F | OA | 83. | 2252 | A9 | 102. | 2265 | 10 |
| 65. | 2240 | A9 | 84. | 2253 | OD | 103. | 2266 | FE |
| 66. | 2241 | OA | 85. | 2254 | FE | 104. | 2267 | 10 |
| 67. | 2242 | FE | 86. | 2255 | OD | 105. | 2268 | 54 |
| 68. | 2243 | OA | 87. | 2256 | 54 | 106. | 2269 | 11 |
| 69. | 2244 | 54 | 88. | 2257 | OE | 107. | 226A | A9 |
| 70. | 2245 | OB | 89. | 2258 | A9 | 108. | 226B | 11 |
| 71. | 2246 | A9 | 90. | 2259 | OE | 109. | 226C | FE |
| 72. | 2247 | OB | 91. | 225A | FE | 110. | 226D | 11 |
| 73. | 2248 | FE | 92. | 225D | OE | 111. | 226E | 54 |
| 74. | 2249 | OB | 93. | 225C | 54 | 112. | 226F | 12 |
| 75. | 224A | 54 | 94. | 225D | OF | 113. | 2270 | A9 |
| 76. | 224B | OC | 95. | 225E | A9 | 114. | 2271 | 12 |
| 77. | 224C | A9 | 96. | 225F | OF | 115. | 2272 | FE |
| 78. | 224D | OC | 97. | 2260 | FE | 116. | 2273 | 12 |
| 79. | 224E | FE | 98. | 2261 | OF | 117. | 2274 | 54 |
| 80. | 224F | OC | 99. | 2262 | 54 | 118. | 2275 | 13 |
| 81. | 2250 | 54 | 100. | 2263 | 10 | 119. | 2276 | A9 |
| 82. | 2251 | OD | 101. | 2264 | A9 | 120. | 2277 | A3 |

In the present work, counter 2 ( of 8253 ) is used in mode 'O'. In this mode, the counter output becomes low as soon as the count is loaded and goes high on terminal count out. The down counting is enabled by the high status of gate. The high going output of the counter 2 interrupts microprocessor via RST 6.5. The moment RST 6.5 is recognised, selected firing command word is outputed to Port A of 8255 PPI.

## 4.3 SYNCHRONIZING AND ZERO CROSSING DETECTOR CIRCUIT

The circuit diagram for zero crossing detection (Base interrupt) and synchronisation ($\phi_R$, $\phi_Y$, $\phi_B$) is given in Fig. 4.4. Line voltages are stepped down and isolated by $\Delta/Y$ connected transformer. The advantage of $\Delta/Y$ connection is that the secondary output voltages will be in phase with line voltages. These a.c. signals are compared with OV in IC 741 comparator. The output signal of comparator is a square wave in phase with line voltages. The signals are reduced to digital TTL level with the help of 5V Zener diode.

In order to obtain 6 signals from 3 digital power signals, $\phi_R$, $\phi_Y$ and $\phi_B$, these signals are inverted using 7404 Hex inverter to get $\overline{\phi}_R$, $\overline{\phi}_Y$, $\overline{\phi}_B$ . The rising edge of these 6 signals are used to trigger 6 monoshots. The six monoshots have been obtained by using three 74121 IC's.The
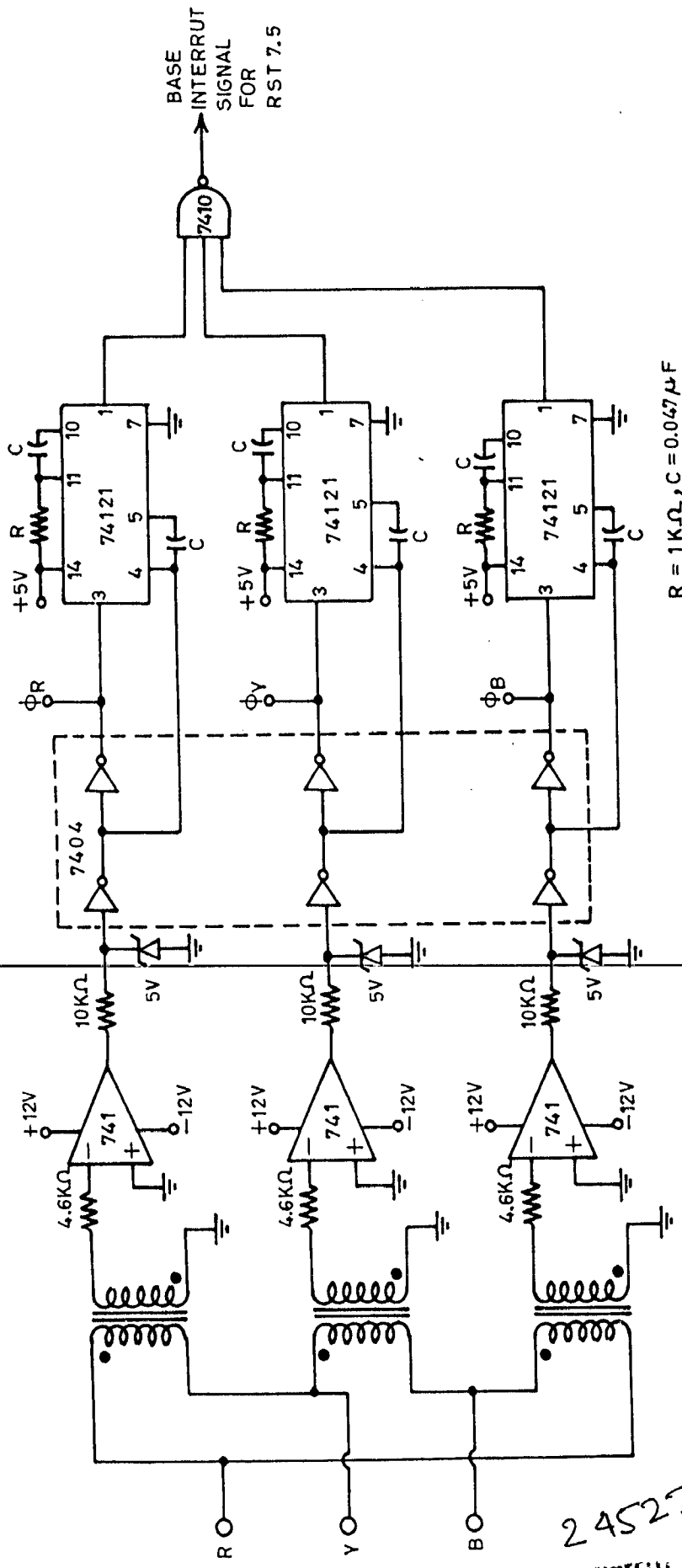
Fig.4.4: Block diagram of zero crossing circuit.

$R = 1 K\Omega, C = 0.047 \mu F$

BASE
INTERRUT
SIGNAL
FOR
RST 7.5

output pulse width of monoshot is decided by the external timing capacitor and resistance and is given by

$$t_w = 0.68 \ R_{ext} \cdot C_{ext}$$

with $R_{ext}$= 1 K ohms and $C_{ext}$ = 0.047 uF

$$t_w = 23 \ u \ sec.$$

Combining these sets of pulse signals, base interrupt is obtained. The utilization of the base interrupt signal for interrupting CPU and for generation of pulses for correct thyristors is explained in the system software implementation [23]. The theoretical wave forms for base interrupt generation circuit are given in Fig. 4.2.

## 4.4 PULSE AMPLIFIER CIRCUIT

The pulses issued from Port-A of 8255 PPI are not strong enough to turn on SCR's. Beside this gate and cathode terminals of SCR are at higher potentials of power circuit and hence control circuit should not be directly connected to the power circuit. A pulse transformer is used to provide physical isolation between the control circuit and the power circuit. The firing pulse from I/O port and an all time high signal (i.e. +5VDC) are ANDED (to avoid up loading), amplified and fed to pulse transformer. A diode is connected across the pulse transformer primary to avoid the saturation of pulse transformer and to protect the transistor against induced over voltage.

Gate protection is required for large reverse voltages and over current. Because of low power level of the control circuitry, this protection can be provided by simple means. The gate can be protected against reverse voltages by connecting a diode across gate and cathode and against over current by connecting a resistance in series with the pulse trans - former. A capacitor is connected across the gate to cathode to bypass the noise pulse. The pulse amplifier circuit is shown in Fig. 4.5.

## 4.5 SYSTEM SOFTWARE IMPLEMENTATION AND FLOW CHARTS

In the following discussion the development of system software and flow charts are presented. In the present work two hardware interrupts are used e.g. RST 7.5 interrupt and RST 6.5 interrupt. The RST 7.5 interrupt is used for base interrupt signal and RST 6.5 interrupt is used for timer interrupt to produce delay proportional to firing angle. The subroutine software programmes have been tested individually on a VMC-85/9 up trainer kit.

### 4.5.1 Main Program Routine

The main program starts with initialization of firing command group pointer and initialization of I/O ports. The I/O ports viz. Port A, Port B and Port C of programmable peripheral interface chip 8255 are initialized, as needed (Port A O/P, Port-B O/P, Port $C_L$ I/P, Port $C_U$ O/P). The RST 7.5 interrupt is unmasked and interrupt system is enabled. Microprocessor waits for the RST 7.5 interrupt in HLT state.
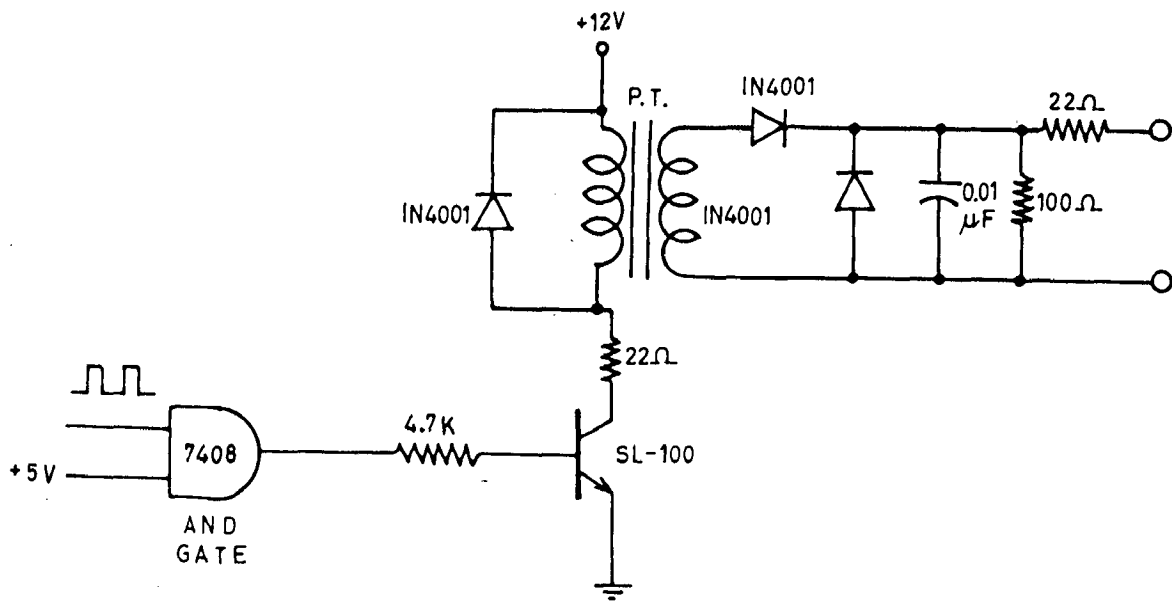
Fig. 4.5: Pulse amplifier.

## 4.5.2 RST 7.5 Subroutine

The moment microprocessor recognises RST 7.5 interrupt it enters into RST 7.5 interrupt service routine. In this routine, counter 2 of timer 8253 is initialized in mode zero. The firing angle is fetched from memory location and is pro - cessed to compute the interval of firing angle i.e. $0-60°$, $60°-120°$ or $120°-180°$. Depending upon the interval of firing angle, firing command pointer is modified and firing angle is adjusted for the range $0-60°$. Since the delay word is of two byte for every firing angle between $0-60°$, the adjusted value of $\alpha$ is doubled to get the LSB of the address for delay word. The MSB is 22H in this program and is loaded into register D. LSB as calculated earlier is taken into register E, and thus register pair DE acts as pointer for delay word. Delay word is loaded from memory location pointed by pointer and pointer+1. The 8253 starts down-counting. In the mean time status of 3 digital signals is inputed and pair of thyristors to be fired for current $60°$ interval is selected. Now on word up waits at HLT state for timer to interrupt via RST 6.5 interrupt.

## 4.5.3 RST 6.5 Subroutine

When the counter 2 of timer reaches terminal count, the output signal of timer becomes high and interrupts up via RST 6.5. In this interrupt service routine, the thyristor pairs selected are fired. A software delay is introduced for

sufficient pulse width to reliably turn on SCR. The gate pulses are then withdrawn and up returns from RST 6.5 routine.

The flow charts for main program , RST 7.5 interrupt service routine and RST 6.5 interrupt service routine are given in Fig. 4.6, 4.7 and 4.8 respectively. The complete program in assembly language is given in Appendix - IV.

## 4.6    RATINGS OF POWER CIRCUIT

The power circuit for the present work consists of following parts.

(i)     Three phase diode bridge

(ii)    Three phase line commutated inverter bridge

(iii)   D.C.link filter.

A power circuit panel has been fabricated to house the rectifier and inverter bridges. The diodes and SCR's have been mounted on heat sinks to dissipate the heat developed. The ratings of diode and SCR's must be such that they should not be exeeeded when maximum power is being delivered. The ratings of diode and SCR's have been selected to 1200V PIV and 16 Amps. Each SCR should be provided with over current, $\frac{di}{dt}$ and $\frac{dv}{dt}$ protections. Over current protection can be provided by connecting a  fuse in series with thyristors. Series connected resister capacitor combination (known as Snubber Circuit) is used against large $\frac{dv}{dt}$ protection. $\frac{di}{dt}$ protection can be provided by placing an inductor having
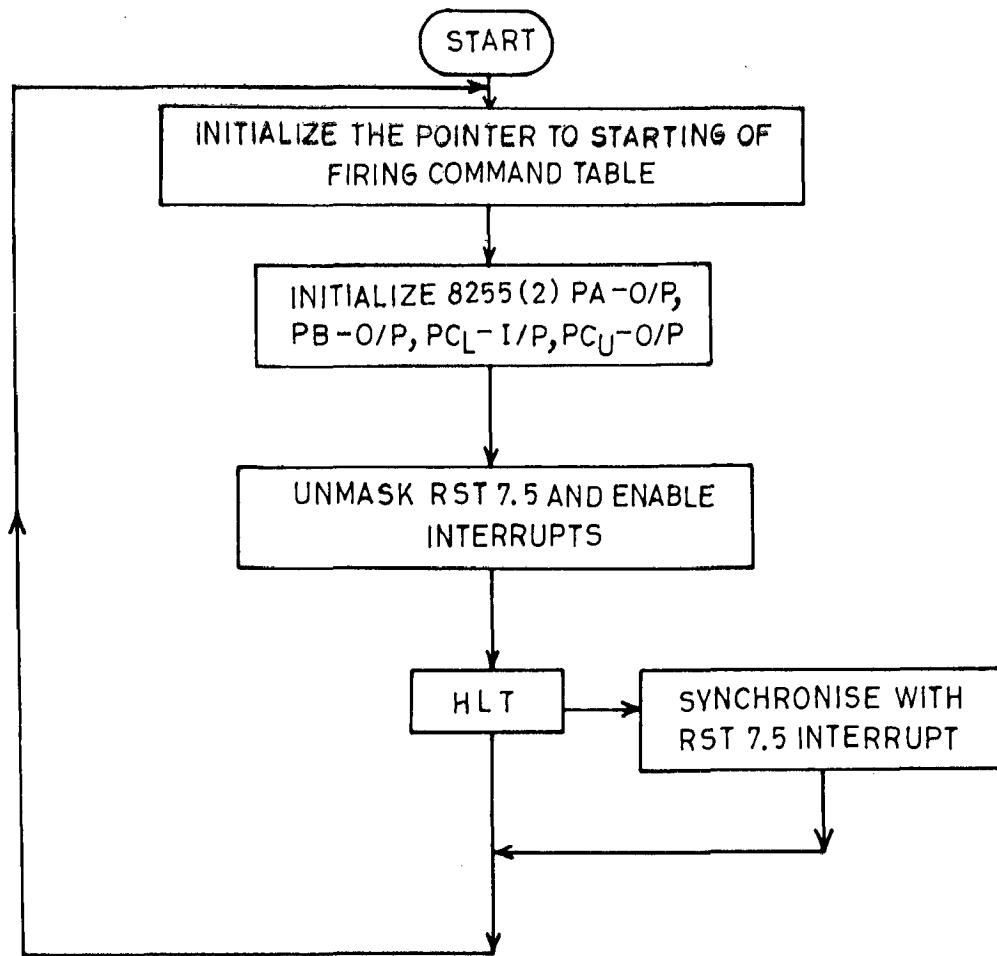
Fig. 4.6: Flow chart for main programme .
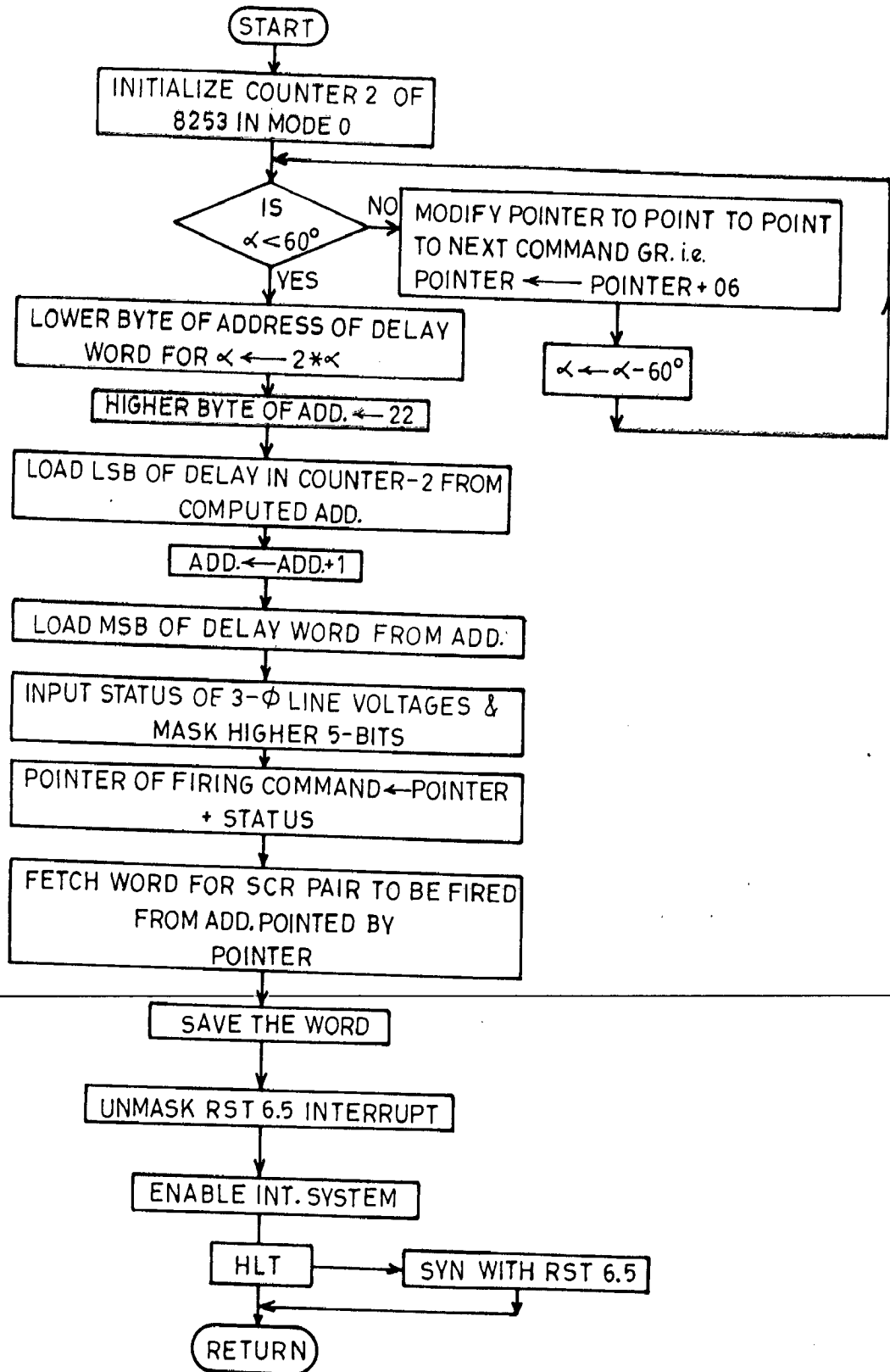
Fig.4.7: Flow chart for RST 7.5 subroutine.
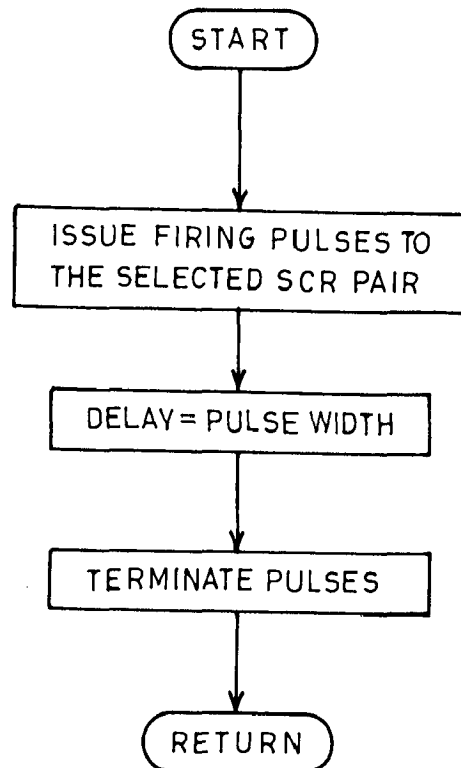
Fig. 4.8: Flow chart for RST 6.5 subroutine.

very low inductance in series with thyristors. An air core inductor has been used as filter for smoothing the dc ripples in the rectifier inverter link.

## 4.7 CONCLUSIONS

In this chapter the line commutated inverter firing scheme using 8085 up has been discussed. Development of various software subroutines along with necessary hardware has been discussed.
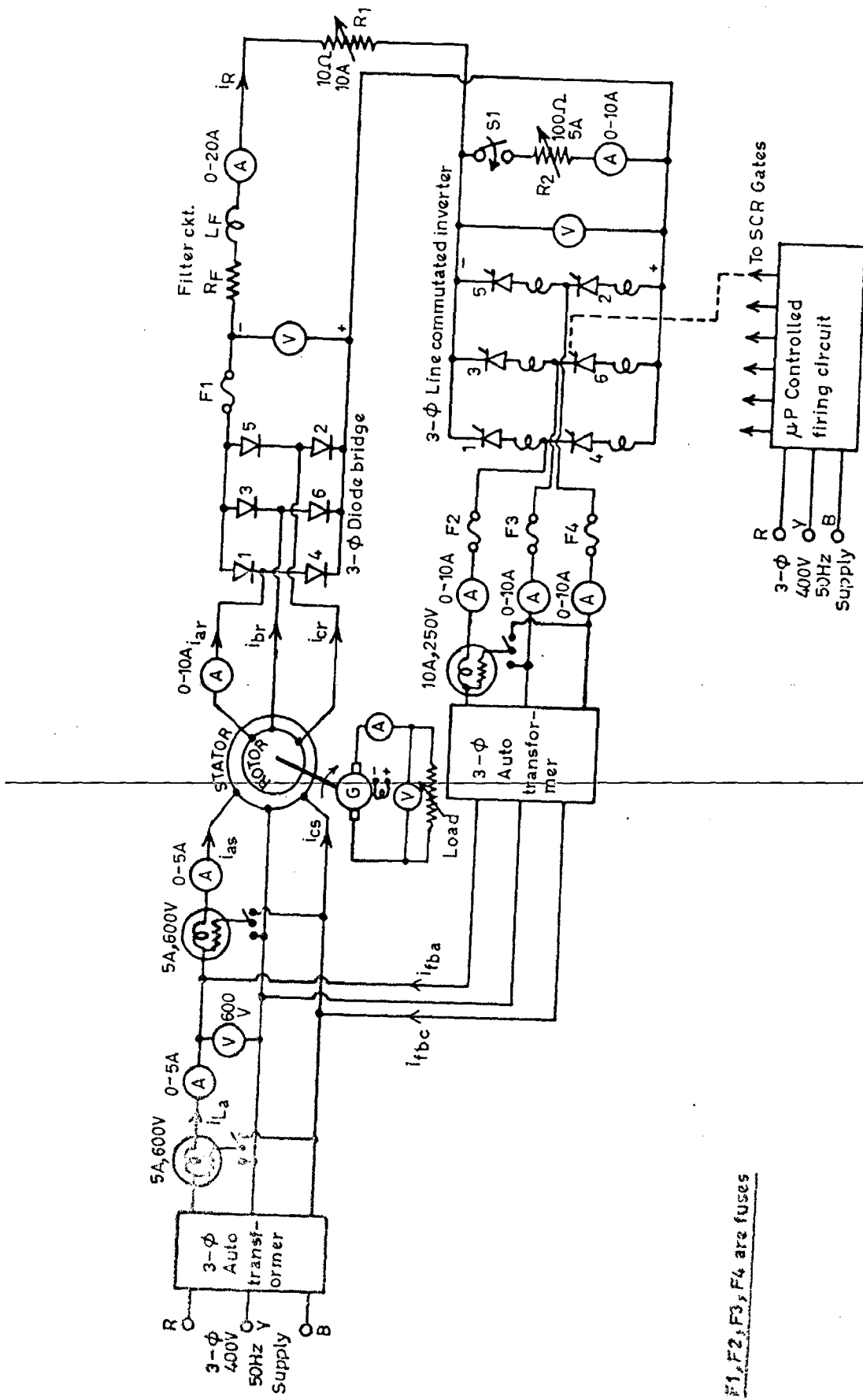
# CHAPTER - V

## EXPERIMENTAL INVESTIGATIONS

### 5.1 INTRODUCTION

The present chapter deals with the experimental investigations on microprocessor controlled static slip power recovery scheme. The results obtained from the experimental investigations have been compared with the analytical results computed in chapter III and the discrepancies between the two are discussed. The oscillograms of supply voltage, supply current, stater voltage, stater current, d.c. link voltage, d.c. link current, inverter a.c. voltage, inverter feedback current, rotor current at different values of firing angle and voltage waveforms at different points of firing control circuit are also presented and discussed.

### 5.2 STARTING OF SLIP POWER RECOVERY DRIVE

Fig. 5.1 gives the circuit diagram of the experimental set up. The switch S1 is closed and then stater is fed from 3-phase auto transformer to the rated voltage and machine is started as a slip ring motor with external resistance in rotor. When the motor picks up speed (which will depend on the series connected resistances R1 and R2), rheostat R2 is increased to full value so that significant d.c. voltage is applied across the inverter. Now the firing pulses from the microprocessor controlled unit are sent to inverter thyristors. When all the three currents on the output side of inverter become equal, it

Fig. 5.1: Experimental set-up.

F1, F2, F3, F4 are fuses

indicates that the inverter has started feeding current to a.c. mains. The switch S1 is now opened and rheostat R1 is cut to zero value. Thus the slip power recovery drive is started and reaches the operating point defined by firing angle and load.

## 5.3 EXPERIMENTAL VERIFICATION OF STEADY STATE PERFORMANCE

To verify the computed steady state performance characteristics, the laboratory tests have been carried out on fabricated system. Drive has been run with different settings of firing angle and experimental performance characteristics have been compared with computed performance curves.

## 5.3.1 Variation of No Load Slip

The variation of no load slip with inverter firing angle is given in Fig. 5.2. The computed curve is shown by solid line whereas the experimental curve is shown by dotted line. From Fig. 5.2 it is observed that the experimental no load slip at a particular setting of inverter firing angle is slightly higher than computed no load slip. This is because of the fact that there is certain torque due to friction. Moreover a 10 HP d.c. machine is coupled with the drive for loading purposes which further increases the no load torque and hence the no load slip. The experimental curve shows a good correlation with the computed one.
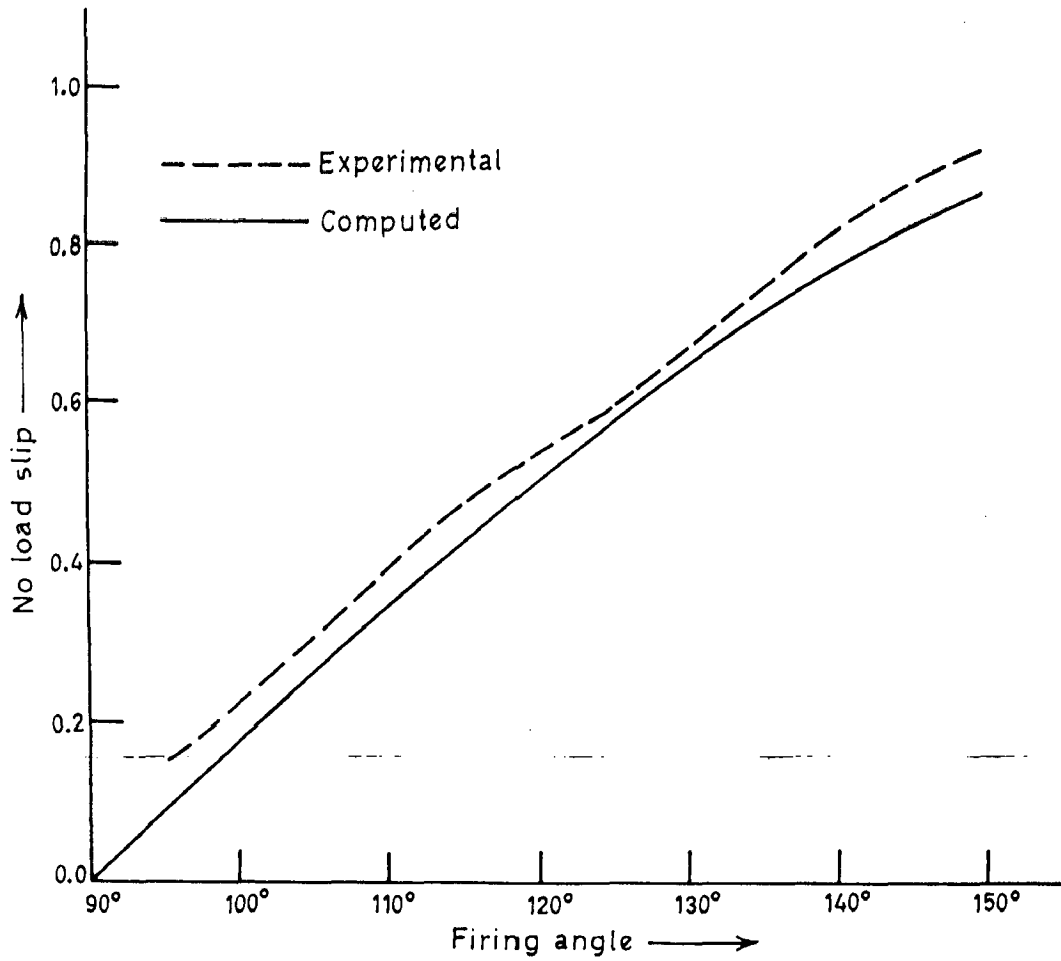
indicates that the inverter has started feeding current
to a.c. mains. The switch S1 is now opened and rheostat
R1 is cut to zero value. Thus the slip power recovery drive
is started and reaches the operating point defined by firing
angle and load.

## 5.3  EXPERIMENTAL VERIFICATION OF STEADY STATE PERFORMANCE

To verify the computed steady state performance
characteristics, the laboratory tests have been carried
out on fabricated system. Drive has been run with different
settings of firing angle and experimental performance cha-
racteristics have been compared with computed performance
curves.

### 5.3.1  Variation of No Load    Slip

The variation of no load slip with inverter firing
angle is given in Fig. 5.2. The computed curve is  shown
by solid line  whereas the experimental curve is  shown by
dotted line . From Fig. 5.2 it is observed that the experi-
mental no load slip at a particular setting of inverter
firing angle is slightly higher than computed no load slip.
This is because of the fact that there is certain torque due
to friction. Moreover a 10 HP d.c. machine is coupled with the
drive for loading purposes which further increases the no
load torque and hence the no load slip. The experimental
curve shows a good correlation with the computed one.

Fig.5.2: No load slip-firing angle characteristics.

5.3.2  Performance Curves at Firing Angle Setting of 95°

Performance characteristics of the drive at firing
angle setting of 95° are shown in Fig. 5.3. Experimental
characteristics and computed characteristics have been
shown  by dotted and solid curves respectively. The no
load speed at firing angle 95° is 1275 r.p.m..Fig. 5.3(a)
shows the experimental and computed torque vs slip charac-
teristics. It is noted that for a given value of slip
computed torque is slightly higher than the torque experi-
mentally obtained. This is because of losses occuring in
the loading d.c. machine. The experimental and computed
characteristics are matching closely. Fig. 5.3(b) shows
the power factor/slip characteristic which indicates that
measured power factor for a given slip is slightly higher
than the computed one. Fig. 5.3(c) shows the efficiency
vs slip characteristics. The curve shows that the experi-
mentally obtained efficiency is slightly lower than computed
efficiency. Fig. 5.3(d) and Fig. 5.3(e) show the supply
current vs slip and torque developed vs d.c. link current at
firing angle setting of 95° respectively. The closeness of
experimental characteristics with computed characteristics
confirms the validity of mathematical model developed for
steady state analysis of slip power recovery scheme.

5.3.3  Performance curves At Firing Angle Setting of 125°

The performance characteristics of the drive at firing
angle setting of 125° are given in Fig. 5.4. The no load
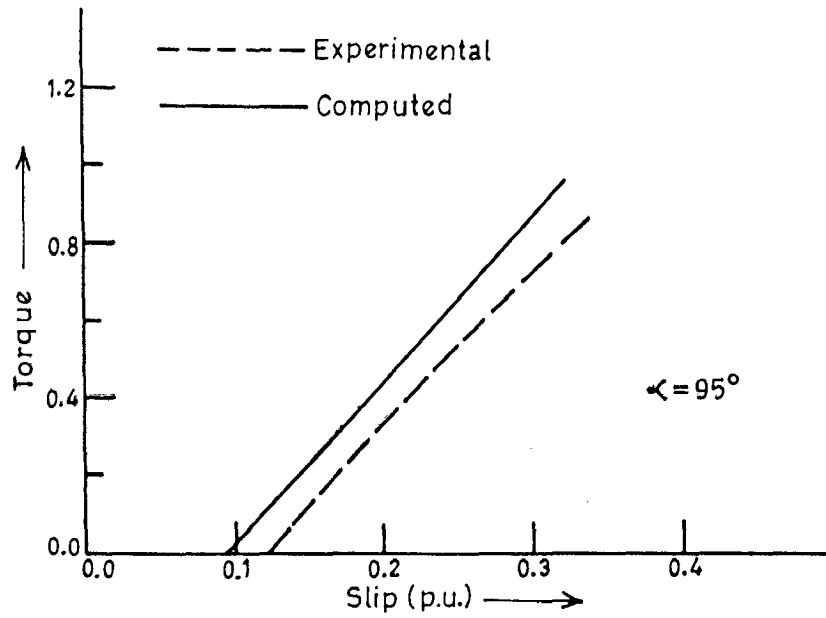
Fig.5.3(a): Torque - slip characteristics.
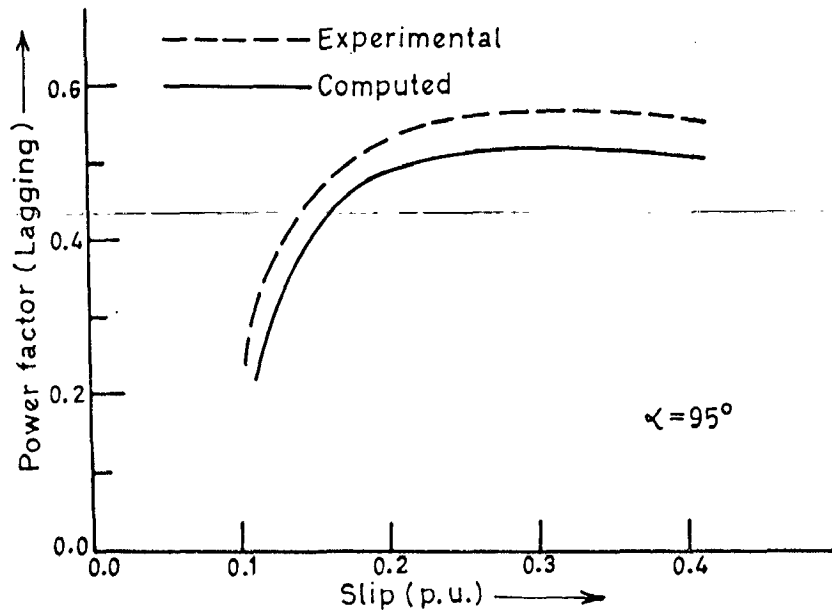


Fig.5.3(b): Power factor -slip characteristics.
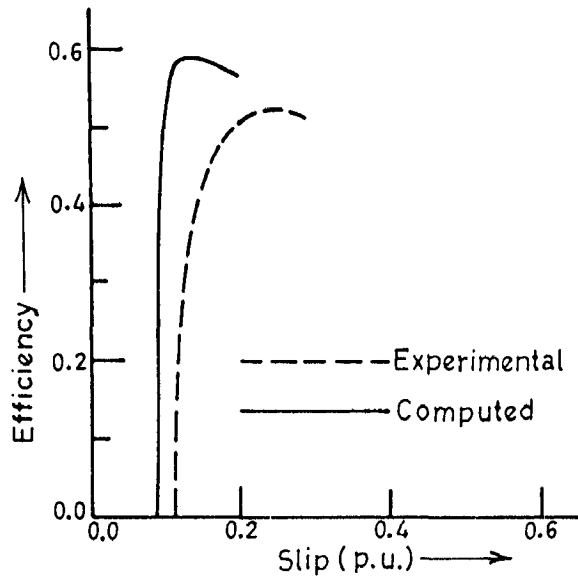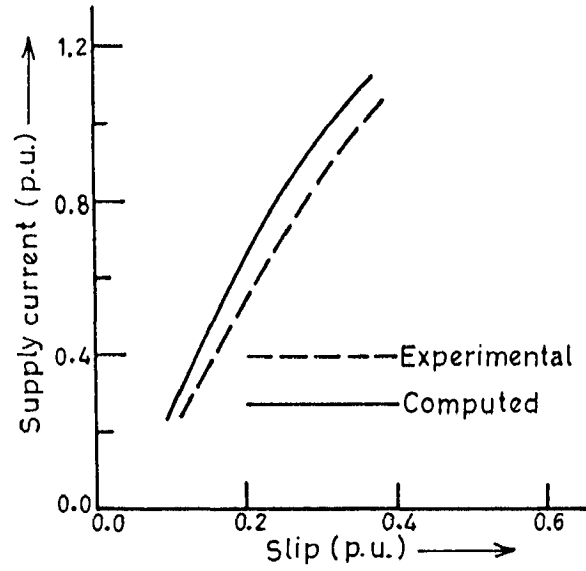
Fig.5.3(c): Efficiency – slip
characteristics.

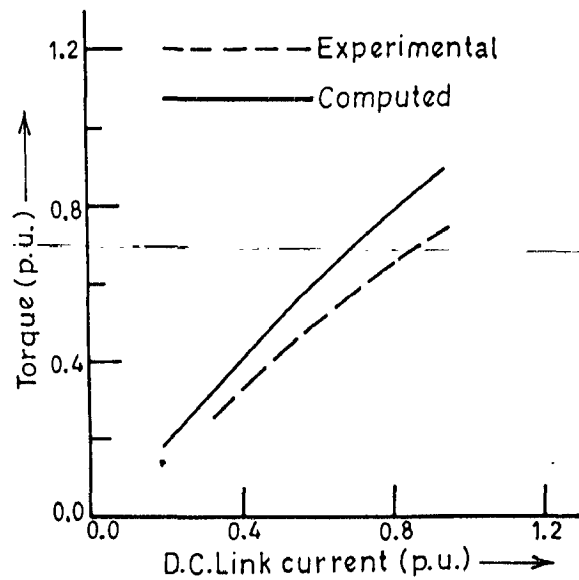Fig.5.3(d): Supply current–slip
characteristics.

Fig.5.3(e): Torque – d.c.link current
characteristics.

Fig.5.3: DIFFERENT PERFORMANCE CHARACTERISTICS
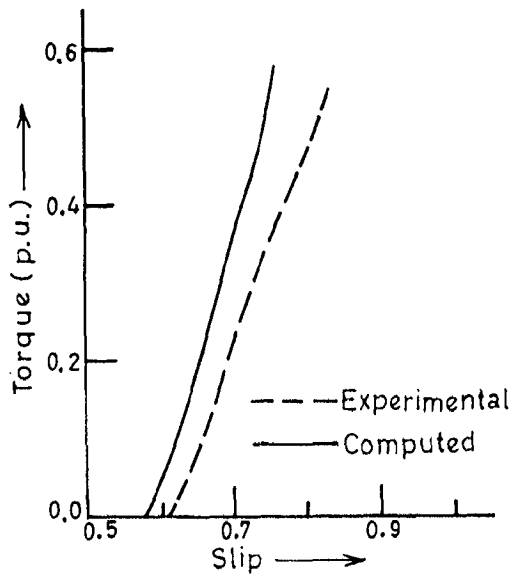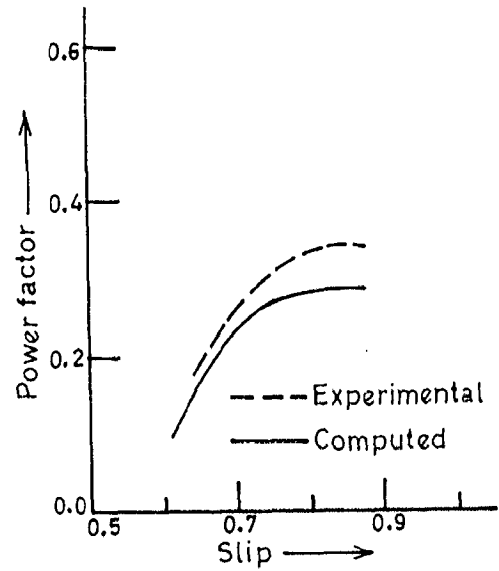AT FIRING ANGLE SETTING OF 95°.

Fig.5.4(a): Torque vs. slip curves.

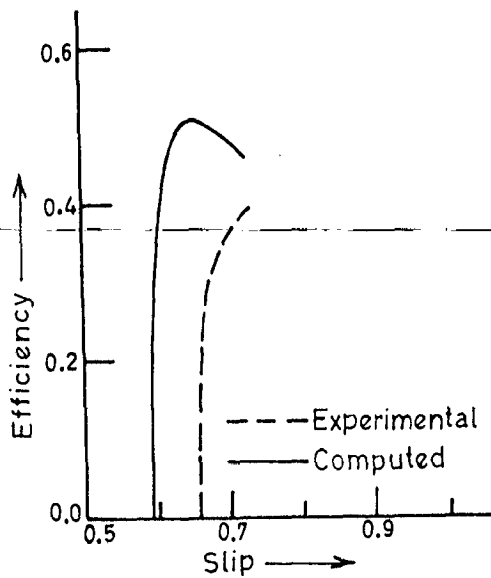Fig.5.4(b): Power factor vs. slip curves.
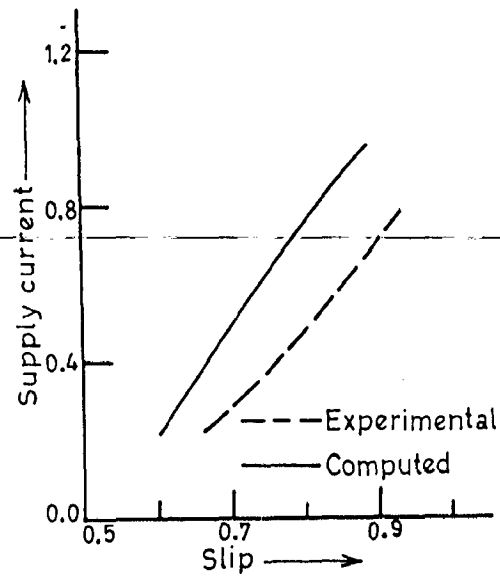
Fig.5.4(c): Efficiency vs. slip curves.

Fig.5.4(d): Supply current vs. slip curves.

Fig.5.4: DIFFERENT PERFORMANCE CURVES AT FIRING ANGLE, $\alpha = 125°$.

speed of the drive at firing angle 125° is 605 r.p.m.

The characteristics of firing angle 125° give the performance of the drive in lower region of speed control range for torque, power factor, efficiency and supply current. In this case too the experimental curves are seen to follow the nature of the computed curves with the trend of discrepancy remaining as before.

5.3.4 Reasons For Discrepancies Between Computed and Experimentally Measured Results.

The discrepancies between the computed and experimentally determined curves may be due to the following reasons -

(i)     In the analysis, it has been assumed that the parameters do not alter with operating conditions of the system. But in practice, some of them may vary with operating conditions of the system.

(ii)    The electrodynamic effects of the harmonics have been neglected in the analysis of the drive.

(iii)   The effect of overlap angle in rectifier and inverter has been neglected.

(iv)    Harmonics in the output current of the inverter have been neglected.

(v)     Instrument errors and errors in recording may also cause some discrepancies.

5.3.5 Discussion on Oscillographic Results

The voltage waveforms at different points of firing control circuit are shown in Fig. 5.5. Fig. 5.5(a) shows the digitized power signal $\phi_R$ derived from the stepped down line voltage $V_{YR}$. The two digitized signals $\phi_R$ and $\phi_Y$ are shown in Fig. 5.5(b) displaced at $120^\circ$. Six base interrupt signals (RST 7.5 interrupt) in one cycle of the supply voltage are presented in Fig. 5.5(c). Fig. 5.5(d) gives the timer output (RST 6.5 interrupt) at every $60^\circ$ interval with digitized power signal $\phi_R$. Fig. 5.5(e) shows the gate pulses to two consequtive SCR's taken at pins PAO and PA1 of I/O 8255. All these waveforms are exactly identical to the theoretical waveforms given in chapter IV.

Fig. 5.6(a) and Fig. 5.6(b) show the rotor current and stator current waveforms respectively when the diode bridge rectifier is connected resistance and inverter is removed. These waveforms correspond to normal induction motor operation. The notches in the rotor current may be attributed to the switching of diodes. The reflection of the same is observed in the stator current shown in Fig. 5.6(b). The neutral of the stator winding has not been connected to the supply neutral therefore, the unbalance, if any, may affect the stator
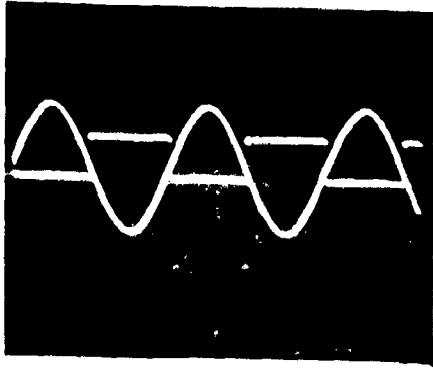
Fig. 5.5(a) Steped down line
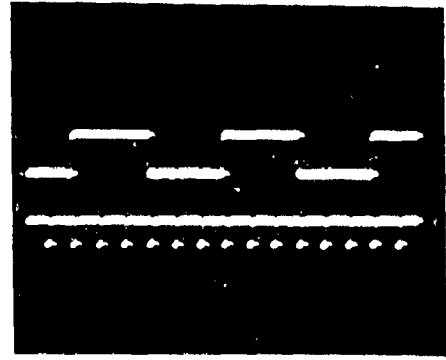voltage $V_{YR}$ and digitized
power signal $\phi_R$



Fig. 5.5(d) Digitized power
signal $\phi_R$ and output of
timer (counter-2) for
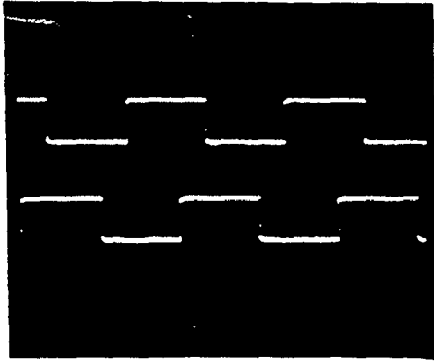RST 5.5 Interrupt



Fig. 5.5(b) Digitized Power
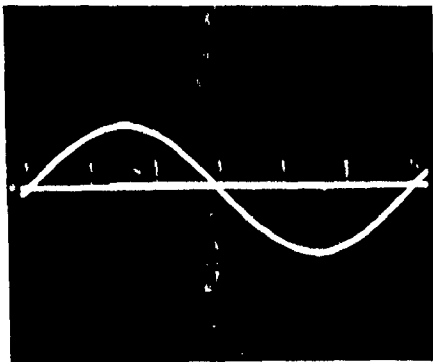signals $\phi_R$ and $\phi_Y$



Fig.5.5(c) Stepped down line
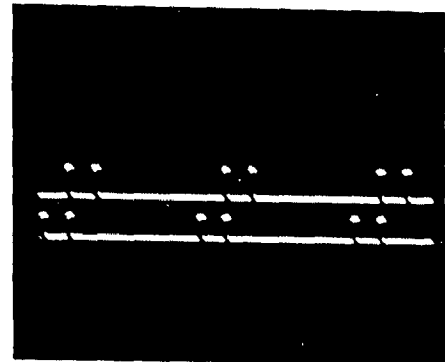voltage $V_{YR}$ and base interrupt
signal



Fig. 5.5(e) Firing pulses
for SCRs 1 and 2 at
PA0-PA1 of 8255.

FIG. 5.5

Various voltage wave forms of firing Circuit
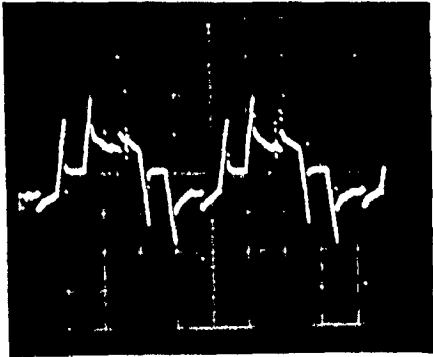
Scale - Horizontal  5m sec/div
        Vertical    5V/div.

Fig. 5.6(a) Rotor current
(2.2 Amps) waveform when
bridge rectifier is closed
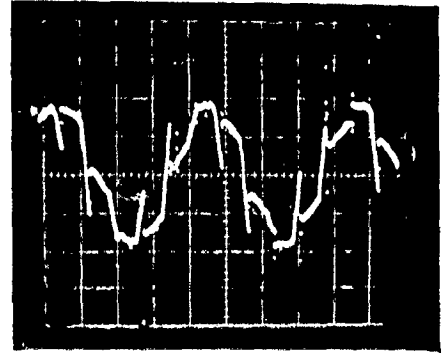through Resistance and
inverter removed.



Fig. 5.6(b) $I_{stator}$= 2.0 Amp.
when bridge rectifier is closed
through Resistance and
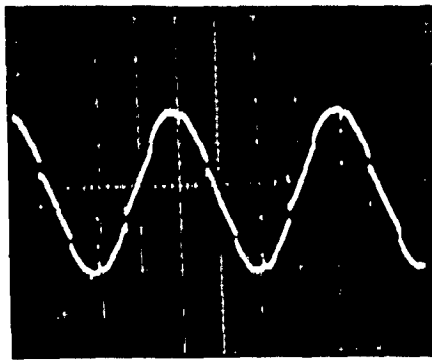inverter removed.



Fig. 5.6(c) Inverter voltage
waveform on a.c. side $(V_{RY})$ at
$\alpha = 130^{0}$.

FIG. 5.6

Typical waveforms for plane induction motor
with diode bridge rectifier in rotor circuit
and inverter voltage waveform at $\alpha =130^{0}$.

Scale -    5 mSec./div.

current waveform. Fig. 5.6(c) shows the inverter voltage waveform (mains side) with very small commutation overlap.

Fig. 5.7 and Fig. 5.8 give oscillograms of voltage/current at various points of the power circuit under two settings of inverter firing angle i.e. $\alpha = 95^\circ$ and $\alpha = 130^\circ$ respectively. The different points selected for oscillo - graphic recording of voltage/current waveform of power circuit are -

(i)     D.C.link current/voltage

(ii)    Rotor current

(iii)   Stator current/voltage

(iv)    Inverter current/voltage

(v)     Supply current/voltage

The d.c. link current ripples under no load and loaded conditions are given in Fig. 5.7(a) and 5.7(b) respectively. The d.c. link current waveform seems to be improved with loading. Fig. 5.7(c) and Fig. 5.7(d) represent rotor currents under unloaded and loaded conditions. It has six spikes in one cycle of rotor frequency. These spikes are due to the switching action of diodes in bridge rectifier. The rotor current distortion may be seen to be reflected on stator current under unloaded and loaded conditions as shown in Fig. 5.7(e) and Fig. 5.7(f) respectively. Under loaded conditions, the stator current
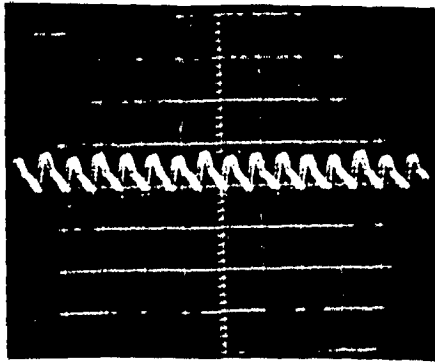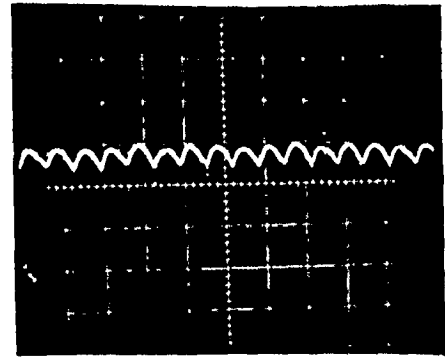
Fig.5.7(a) $I_{d.c.link}=4.3A$
under no load.



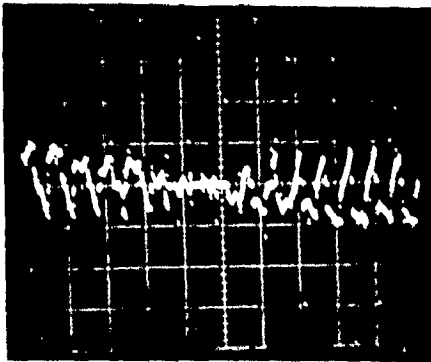Fig. 5.7(b) $I_{d.c.link}=3.2A$
under loaded condition.



Fig.5.7(c) $I_{rotor}=2.0A$
under no load
speed = 1275 rpm.
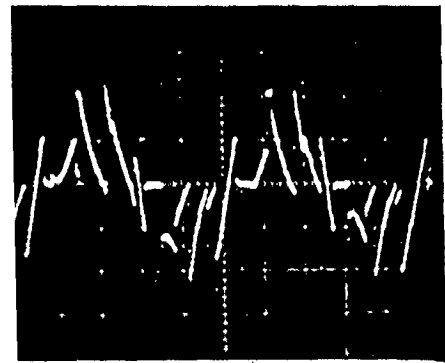


Fig.5.7(d) $I_{rotor}=5.5A$
under loaded condition
speed = 629 rpm.
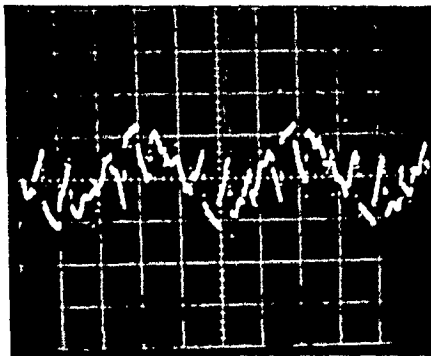


Fig.5.7(e) $I_{stator}=1.2A$
under no load
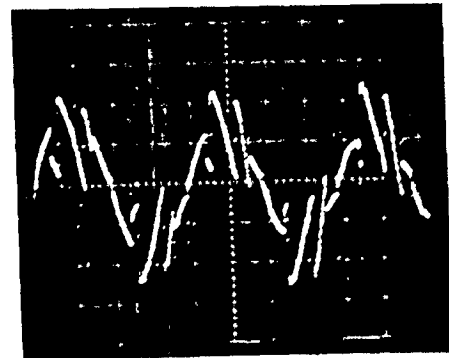


Fig.5.7(f) $I_{stator}=3.3A$
under loaded condition.
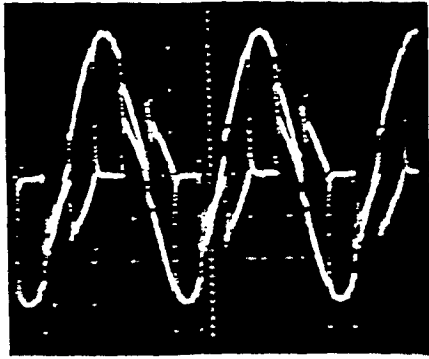
Fig.5.7(g) $V_{inv.}$=190V (L-L)
$I_{inv.}$ = 3.3A under no load



Fig.5.7(h) $I_{inv.}$=6.5A
under loaded condition



Fig.5.7(i) $V_{supply}$= 400 V
$I_{supply}$ = 1.4A
under no load.



Fig.5.7(j) $V_{supply}$=400 V
$I_{supply}$ = 4.1 A
under loaded condition

FIG. 5.7

Different voltage/current oscillograms
under no load and loaded condition at
firing angle $\alpha$= 95°.

Scale   5 m sec/div.
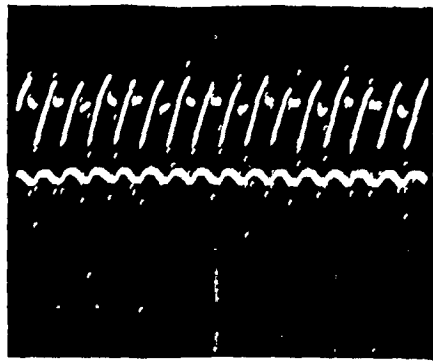
Fig.5.8(a) $V_{d.c.link}=148$ V
$I_{d.c. link}=1.2$ A
under no load.
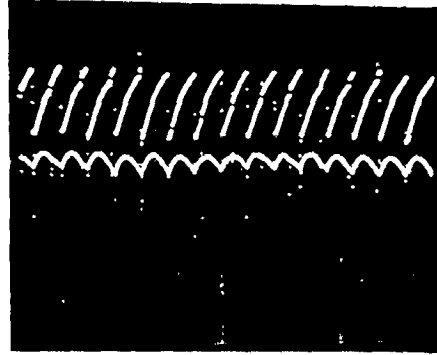


Fig. 5.8(b) $V_{d.c.link}=180$ V
$I_{d.c.link} = 3.6$ A
under loaded condition.
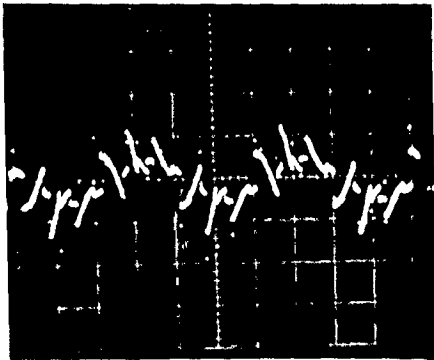


Fig.5.8(c) $I_{stator}=1.2A$
under no load.
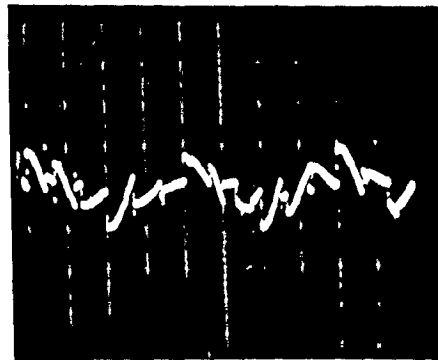


Fig. 5.8(d) $I_{stator}=2.9$ A
under loaded condition.
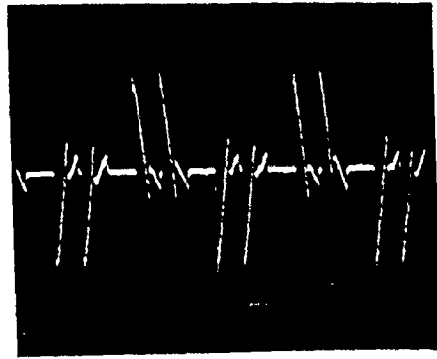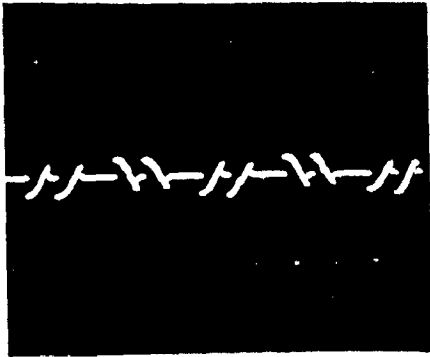
Fig.5.8(e) $I_{inv.}$=0.8 A
under no load.
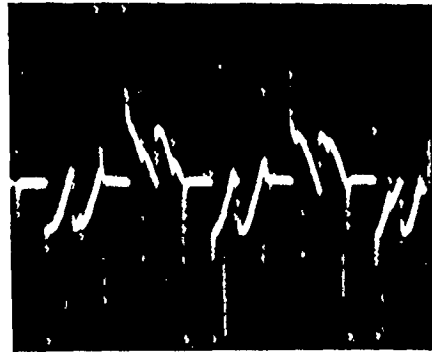


Fig.5.8(f) $I_{inv.}$=4.1 A
under loaded condition.

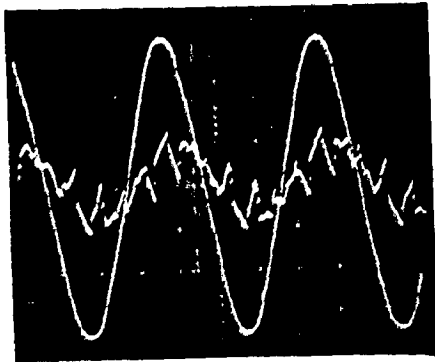

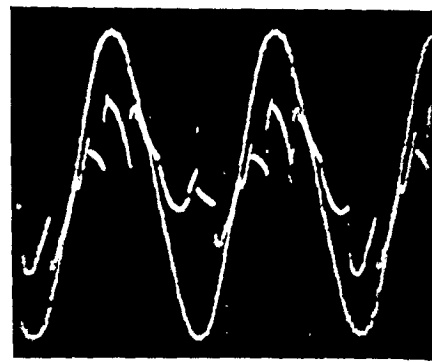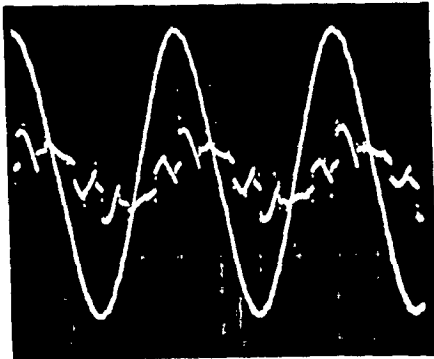Fig.5.8(g) $V_{supply}$=400 V
$I_{supply}$ = 1.4 A
under no load.
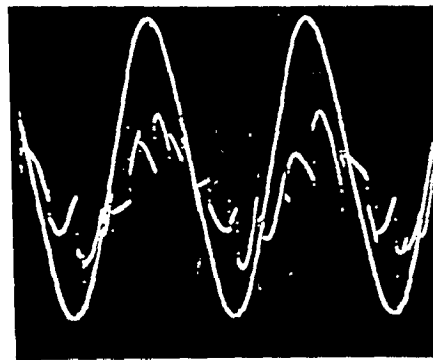


Fig.5.8(h) $V_{supply}$=400 V
$I_{supply}$ = 2.6A
under loaded condition.

FIG. 5.8

Typical voltage/current oscillograms
at firing angle $\alpha$ = 130°.
Scale   5 m sec./div.

waveform improves slightly. Fig. 5.7(g) and Fig. 5.7(h) shows the inverter voltage and current waveforms under unloaded and loaded condition respectively. The inverter current waveform is not continuous over the $120^{\circ}$ condition period. The supply current/voltage waveforms under unloaded and loaded conditions are given by Fig. 5.7(i) and Fig. 5.7(j) respectively. The distortion of the supply current may be attributed to

(i)    Distortion in stator current waveform

(ii)   Inverter current does not retain the continuous conduction through out the conduction period.

At firing angle setting of $130^{\circ}$, the voltage and current waveforms are similar to those for firing angle setting of $95^{\circ}$.

5.4    CONCLUSIONS

In this chapter, experiments conducted on the fabricated slip power recovery drive are reported. Load tests at different settings of firing angle have been carried out and the performance curves plotted. They are seem to compare closely in nature and magnitude with the predicted results under corresponding operating conditions. The oscillographic records of control circuit and power circuit are also presented. It is found that the oscillograms of firing control circuit match exactly with the

expected ones where as in the case of power circuit
the oscillograms of voltage/ current at various points
match closely with the expected waveforms. The devia-
tion in voltage/ current waveforms from the ideal
waveforms is chiefly due to appearance of spikes
resulting from switching actions in diode bridge
rectifier.

The drive is found to offer wide range (1300
r.p.m. to 100 r.p.m) of speed control in subsynchronous
range. There are no apparent problems in loading the
drive at any setting of firing angle.

# CHAPTER VI

## CONCLUSIONS AND SUGGESTIONS FOR FURTHER WORK

### 6.1    MAIN CONCLUSIONS

The work presented in the dissertation covers
the (1) design and fabrication of a microprocessor
controlled firing scheme for line commutated inverter
(2) predetermination of steady state performance  and
(3) experimental investigations under steady state of
constant torque type slip power recovery scheme. The
main conclusions of the present work are summarised as
follows -

(i)    The mathematical model developed is simple
and can be used to determine steady state as well
as dynamic performance of the drive in terms of
normal measurable parameters.

(ii)    The investigations show that a wide range of
speed control is possible by varying only one
single parameter i.e. inverter firing angle.

(iii)  The study reveals that the efficiency of the
drive is much more improved in the lower regions
of speed control operation.

(iv)   From the performance characteristics it is seen
that the slip recovery drive exhibit the
characteristic similar  to that of a separately
excited d.c. motor.

(v) From the experimental investigations, it is observed that the system is stable at no load as well as under loaded conditions.

(vi) The computed results and experimentally determined results are in good correlation, thus establishing the validity of developed mathematical model.

## 6.2 SUGGESTIONS FOR FURTHER WORK

During the course of investigation, some problems have arisen which require further investigation. This work may be extended on the following aspects -

(i) In the present work magnetic saturation effect, inverter losses, losses in diode bridge etc. have been neglected to simplify the derivations for development of mathematical model of the drive. The effect of these factors on the drive performance may also be studied.

(ii) The present drive is suitable for open loop control of speed. The closed loop control system may be designed for the drive to achieve better speed regulation.

(iii)   The effect of harmonics on the steady
        state performance of the drive may be
        studied.

(iv)    Speed control in super synchronous region
        may be realized by replacing the diode
        bridge with a fully controlled bridge.
        The present approach can be extended to
        study the behaviour of such a system.

# REFERENCES

1. Openshaw Taylor, E., 'The performance and design
   of A.C.commutator Motors' (book), Sir Isaac Pitman
   and Sons Ltd., London, 1958.

2. Nehrir, M.H., 'Speed Control of 3-phase induction
   motor by stator voltage control', IEEE Trans. on
   Industrial Electronics and Control Instrumentation
   Vol. IECI-22, No.2, pp.172-174, May, 1975.

3. Berg, G.J., Sarkar, A.K., 'Speed Change of induc-
   tion motor with variable frequency supply', IEEE
   Trans. on Power Apparatus and Systems, Vol. PAS-90,
   No.2, pp. 500-508, March-April 1971.

4. Bedford, R.E., Padhye, S.S., 'Computational
   Techniques in determining stability limit of inverter-
   fed. induction motor', Journal IE(I), Part EL3, Vol.56,
   pp. 117-25, Dec. 1975.

5. Paresh, C. Sen, 'Rotor chopper control for induction
   motor drive', IEEE Trans. on Industry Applications,
   Vol. IA-11, No.1, pp.43-49, Jan-Feb., 1975.

6. Shepherd, W., Stanway, J., 'Slip power recovery in
   an induction motor by the use of a thyristor inverter',
   IEEE Trans. on Industry and General Applications,
   Vol. IGA-5, No.1, pp.74-82, Jan./Feb., 1969.

7.  Shepherd, W., Khalil, A.Q., "Capacitive compensation of thyristor-controlled slip energy recovery system, Proceedings IEE, Vol. 117, No.5, pp.943-956, May 1970.

8.  Lavi, A., Polge, R.J., 'Induction motor speed control with static inverter in the rotor', IEEE Trans. on Power Apparatus and Systems, Vol. PAS-85, No.1, pp.76-84, Jan. 1966.

9.  Erlicki, M.S., 'Inverter rotor drive of an induction motor', IEEE Trans. on Power Apparatus and systems, Vol. PAS-84, No.11, pp.1011-1016, Nov. 1965.

10. Mittle, V.N., Venkatesan, K., Gupta, S.C., 'Predetermination of steady state performance of thyristor controlled slip energy recovery system', JIE (India), Vol. 59, pt.EL. pp. 95-99, Oct. 1978.

11. Gupta, S.P., Venkatesan, K., 'Switching transients in static scherbius drive', JIE(India), Vol.60, Pt. EL6, pp. 255-261, June 1980.

12. Hylander, J., Hallenius, K-E., 'Reduction of torque pulsations in an induction machine with a slip power recovery static converters in the rotor circuit', Proc. of ICEM, Munich, part-3, pp. 868-871, Sept.1986.

13. Subrahmanyam, V., Surendran, K., 'Analysis of a variable speed induction motor drive employing static slip energy recovery scheme, Proc. of the ICEM, Munich, part-3, pp.888-891, Sept. 1986.

14. Olivier, G., Stefanovic, V.R., April, G.E.,
'Evaluation of phase commutated converters for
slip power control in induction drives', IEEE Trans.
on Industry Applications, Vol. IA-19, No.1, Jan./
Feb. 1983.

15. Drury, W., Jones B.L.,Brown,J.E. 'Application of
controlled flywheeling to the recovery bridge of a
static Kramer drive,' IEE Proc. Vol. 130, Pt.B, No.2,
March 1983.

16. Taniguchi, K.,Takeda, Y., Hirasa, T., "High per-
formance slip power recovery induction motor', IEE
Proc. Vol. 134, Pt.B, No.4, July 1987.

17. Bose, B.K., 'Adjustable speed A.C.drives - A
Technology status review', Proceedings of IEEE,Vol.70,
No.2, Feb. 1982.

18. Mittle, V.N.,Venkatesan, K., Gupta, S.C.,'Stability
analysis of a constant torque static slip power
recovery drive', IEEE Trans. on Industry Applications,
Vol. IA-16, No.1, pp.119-126, Jan./Feb. 1980.

19. Mittle, V.N., 'Steady state and transient analysis
of a Static Slip-Energy-  Recovery drive', Ph.D.
Thesis, Deptt. of Electrical Engg., Univ. of Roorkee,
Roorkee (India).

20. Surendran, K., Subrahmanyam, V., 'Stability analysis of an induction motor with a converter cascade in the rotor circuit using D-Decomposition method', Proc. of the ICEM, Munich, Part-3, pp.892-895, Sept. 1986.

21. Bird, B.M., Mehta, P., 'Regenerative braking in slip power-recovery systems', Proc. IEE, Vol. 119, No.9, pp. 1343-1344, Sept. 1972.

22. Bland, T.G., Shepherd, W., 'Controlled braking of slip energy recovery drive utilizing capacitor excitation of induction motor', IEEE Trans. on Industrial Electronics and Control Instrumentation, Vol. IECI-22, No.2, pp. 208-13, May 1975.

23. Tang, P.C., Lu, S.S., Wu, Y.C., 'Microprocessor Based design of a firing circuit for three phase full-wave thyristor dual converter', IEEE Trans. on Industrial Electronics, Vol. IE-29, No.1, pp.67-73, Feb.1982

24. Krause, P.C., Thomas, C.H., 'Simulation of symmetrical induction machinery', IEEE Trans. on Power Apparatus and Systems Vol. PAS-84, No.11, pp. 1038, Nov.1965.

25. Fitzerald, A.E., Kingsley, C., 'Electrical machinery', (Book), McGraw Hill, New York, 1952.

26. Mittal, P., 'Stability analysis of slip energy recovery drive', M.E.Dissertation, Deptt. of Electrical Engg., Univ. of Roorkee, Roorkee (India).

27. Ramamoorthy, M., 'An introduction to thyristors and their applications', (Book), East-West press, New Delhi- Madras, 1972.

28. Murphy, J.M.D., 'Thyristor control of A.C.Motors', (Book), Pergamon Press, 1973., Oxford, England.

29. User's Manual for VMC-85/9, Microprocessor Training/ Development Kit, M/S Vinytics, New Delhi.

30. Intel Component Data Catalog, 1979.

31. Short, K.L., Microprocessor and programmed logic', (Book), Prentice Hall, 1981.

# APPENDIX - I

## SPECIFICATIONS OF INDUCTION MOTOR,
## LOADING D.C.MACHINE AND BASE VALUES

1.  Detailed specifications of slip ring induction

    motor:

    E.M.F.INDUCTION MOTOR

    Made in India.

    Machine No. 23114

    | Volts 400/440V | PH 3, | CY 50 | CON Y |
    | --- | --- | --- | --- |
    | KW 2.2 | H.P.3, | R.P.M. 1440 | |
    | Amps 4.5 | Rotor volts 210V, Rotor Amps 6 | | |
    | Rating CONT, | Class of Insulation 'A' | | |

2.  Specifications of Loading d.c. Machine

    The British Thomson-Houston Co.Ltd.

    Rugby, England

    TYPE DY 3420, COMP, 220 Volts, 40.5 Amps.

    Sl.No. 54434 F, 10 H.P., R.P.M. 1000

    CONT.Rating Brush 1/517.

3.  Base values for Various quantities

    Unit current = Peak value of rated current =6.36A

    Unit voltage = Peak value of rated phase voltage

    = 326.5 V.

    Unit impedance $= \dfrac{\text{Unit voltage}}{\text{Unit current}} = \dfrac{326.5}{6.36}$

    $= 51.3352$

Unit Power = Rated apparent power $= \frac{3}{2}$ x 326.5 x 6.36

$$= 2.49 \text{ KW}$$

Unit frequency = Rated frequency = 50 Hz

Unit electrical angular speed = $2\pi f_b = 100\pi$ rad/sec.

Unit mechanical speed = $\pi f_b$ = $50\pi$ rad/sec.

Unit torque $= \dfrac{\text{Unit power}}{\text{Unit mechanical speed}}$

$$= \dfrac{2.49 \times 10^3}{50 \pi}$$

$$= 15.85 \text{ N-m.}$$

# APPENDIX - II

## PARAMETERS OF DRIVE

### 1. ACTUAL VALUES OF PARAMETERS

The values of measured parameters of the three phase induction motor are as follows.

$X_{ss} = 160.9$ ohms $\qquad R_{ss} = 4.6$ ohms

$X_{rr} = 36.48$ ohms $\qquad R_{rr} = 1.676$ ohms

$X_M = 154$ ohms $\qquad R_F = 0.6$ ohms

$a = 2.1$ $\qquad a_T = 0.48$

$\qquad\qquad\qquad\qquad R'_{rr} = 7.39$ ohms

$\qquad\qquad\qquad\qquad R'_F = 2.46$ ohms

$\qquad\qquad\qquad\qquad X'_{rr} = 160.9$ ohms.

### 2. PER UNIT VALUES OF PARAMETERS

Parameters when expressed in per unit form are as follows.

$R_{ss} = 0.09$ $\qquad R'_{rr} = .14$ $\qquad R'_F = 0.05$

$X_{ss} = 3.1$ $\qquad X'_{rr} = 3.1$ $\qquad X_M = 3.0$

# APPENDIX-III

START

READ DRIVE PARAMETERS
$R_{ss}, R_{rr}, R_F, X_{ss}, X_{rr}, X_M, V_{SM}, a, a_T$

READ VALUES OF SLIP INTERVAL D S
$\propto$ INTERVAL D$\propto$

SET
$\propto = 90°$

COMPUTE NO
LOAD SLIP $S_{nl}$

SLIP $= S_{nl} + DS$

IS
SLIP
$\leq 1$

NO

YES

COMPUTE STEADY STATE VALUES OF $i_{rmo}, \propto_{ro}, i_{dso},$
$i_{qso}, i_{dro}, i_{qro}, T_{eo}, I_{Lo}, PF, i_{RO}, P_i, P_o$ AND EFFICIENCY

SLIP $=$ SLIP $+$ DS

$\propto = \propto + D\propto$

IS
$\propto \leq 180°$

YES

NO

STOP
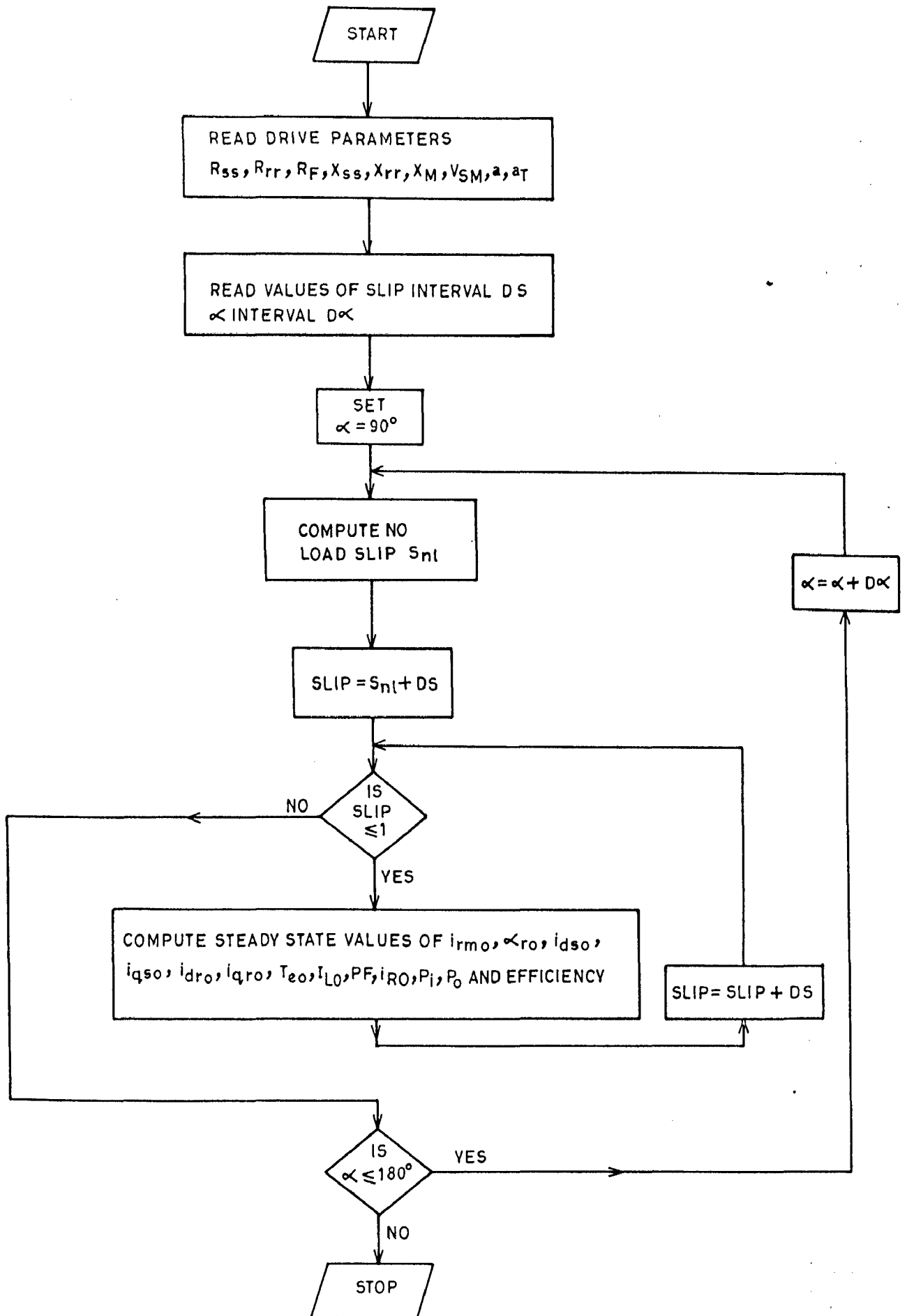
Flow chart for computing steady state performance

```
C       A PROGRAM FOR STUDY STATE SOLUTION
        COMPLEX E,F,G,Y
        OPEN(UNIT=1,FILE='PANDEY.DAT')
        OPEN(UNIT=2,FILE='DUPL.RES')
        READ(1,*) XSS,XRR,XM,RSS,RRR,RF,A,VSM,DALF,DS,AT
        WRITE(*,*)'   ALF    S    TORQ    AISM    AILRMS    PF    EFFY
       1 AIR'
        WRITE(2,*)    ALF    S    TORQ    AISM    AILRMS    PF    EFFY
       1 AIR'
        PI=4*ATAN(1.0)
        ALF=90.
        DO 500 NALF=1,20
        ALFA=ALF*PI/180.
        SNL=A*AT*COS(PI-ALFA)
        SLIP=SNL+.02
        DO 400 S=SLIP,1.0,DS
        Z1=S*XM*VSM/SQRT(RSS*RSS+XSS*XSS)
        Z2=A*VSM*COS(PI-ALFA)*AT
        Z3=RRR+(PI*PI*RF)/18.+(XM*XM*S*RSS)/(RSS*RSS+XSS*XSS)
        Z4=S*XRR-(XSS*XM*XM*S)/(RSS*RSS+XSS*XSS)
        Z5=Z3*Z3+Z4*Z4
        Z6=2.*Z2*Z3
        Z7=Z2*Z2-Z1*Z1
        AIRM=(-Z6+SQRT((Z6*Z6)-(4.*Z5*Z7)))/(2.*Z5)
        AR=((Z4*AIRM)/(Z2+Z3*AIRM))
        ALFR=(PI/2.)-ATAN(XSS/RSS)-ATAN(AR)
        AI=RRR+(PI*PI*RF)/18.
        B=A*AT*VSM*COS(PI-ALFA)+AIRM*AI
        C=S*XRR*AIRM
        D=S*XM
        E=CMPLX(B,C)
        F=CMPLX(COS(ALFR),SIN(ALFR))
        G=CMPLX(0.,D)
        Y=E*F/G
        AISM=CABS(Y)
        AIS=AISM/SQRT(2.)
        PHI=ATAN(AIMAG(Y)/REAL(Y))
        AIDS=AISM*COS(PHI)
        AIQS=AISM*SIN(PHI)
        AIDR=AIRM*COS(ALFR)
        AIQR=AIRM*SIN(ALFR)
        TORQ=XM*(AIDS*AIQR-AIQS*AIDR)
        AIDI=AIRM*COS(PI-ALFA)
        AIL=SQRT((AIDS-AIDI)**2+(AIQS+AIDI*TAN(ALFA))**2)
        AILRMS=AIL/SQRT(2.)
        PF=(AIDS-AIDI)/AIL
        PWIN=(3./2.)*VSM*AIL*PF
        PWOP=(1.-S)*TORQ
        EFFY=PWOP/PWIN*100.
        AIR=0.9067*SQRT(AIDR*AIDR+AIQR*AIQR)
        PLST=RSS*(AIDS*AIDS+AIQS*AIQS)
        PLRT=RRR*(AIDR*AIDR+AIQR*AIQR)
        WRITE(*,15) ALF,S,TORQ,AISM,AILRMS,PF,EFFY,AIR
        WRITE(2,15) ALF,S,TORQ,AISM,AILRMS,PF,EFFY,AIR
400     CONTINUE
        ALF=ALF+DALF
500     CONTINUE
15      FORMAT(1X,F6.2,1X,F6.4,1X,F6.4,1X,F6.4,1X,F6.4,1X,F6.2,1X,F9.4,1X
       1,F6.3)
        STOP
        END
```

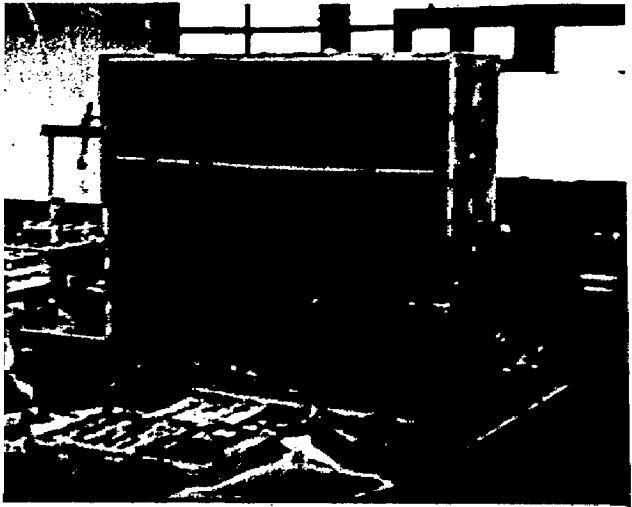| | | | | |
|---|---|---|---|---|
| FUNCTION NAME | | LCI CON | | |
| INPUT | | MEMORY LOCATION 2501 H, 2200H - 2277H, 2101H-2112H | | |
| OUTPUT | | NONE | | |
| CALLS | | NONE | | |
| DESTROYS | | A,B,C,D,E,H,L | | |
| DESCRIPTION | | THIS PROGRAM CONTROLS FIRING ANGLE OF LCI AND THE SEQUENCE OF THE FIRING PULSES TO VARIOUS SCRs FOR EVERY SLOT OF FIRING ANGLE (0-60°, 60°-120°, 120°-180°). | | |

| LEBEL | ADDRESS | CONTENTS | MNEMONICS AND OPERANDS | COMMENTS |
|---|---|---|---|---|
| LCICON | 2000 | 21 00 21 | LXIH 2100 | |
| | 2003 | 22 03 25 | SHLD 2503 | |
| | 2006 | 3E 81 | MVI A, 81 | INITIALIZE 8255(1) MODE 0 |
| | 200B | D3 0B | OUT 0B | PA-O/P, PB - O/P $PC_L$ -I/$P_L$ PCU-O/P |
| | 200A | 3E 1B | MVI A, 1B | UNMASK RST 7.5 |
| | 200C | 30 | SIM | |
| | 200D | FB | EI | |
| | 200E | 76 | HLT | SYN WITH RST 7.5 |
| | 200F | C3 00 20 | JMP 2000 | |
| ISS RST 7.5 | 2012 | 3E B0 | MVI A,B0 | INITIALIZE COUNTER-2 MODE-0 |
| | 2014 | D3 13 | OUT 13 | |
| | 2016 | 21 01 25 | LXIH 2501 | $\alpha$ IN ACCUMULATOR |
| | 2019 | 7E | MOV A,M | |
| | 201A | 23 | INXH | |
| | 201B | 46 | MOV B,M | 60° IN B |
| | 201C | 23 | INX H | |

| LEBEL | ADDRESS | CONTENTS | MNEMONICS AND OPERANDS | COMMENTS |
|---|---|---|---|---|
| | 201D | B8 | CMP B | IS $\alpha < 60^\circ$ |
| | 201E | DA 2D 20 | JC 20 2D | |
| | 2021 | 5F | MOV E,A | SAVE $\alpha$ IN E |
| | 2022 | 3E 06 | MVI A,06 | POINTER OF FIRING COMMAND WORD |
| | 2024 | 86 | ADD M | MODIFIED TO POINT TO THE NEXT COMMAND GROUP |
| | 2025 | 00 | NOP | |
| | 2026 | 77 | MOV M,A | POINTER=POINTER+06 |
| | 2027 | 7B | MOV A,E | |
| | 2028 | 90 | SUB B | $\alpha - \alpha-60^\circ$ |
| | 2029 | 00 | NOP | AGAIN CHECK VALUE OF $\alpha$ LESS THAN $60^\circ$ |
| | 202A | C3 1D 20 | JMP 201D | |
| | 202D | 87 | ADD A | $\alpha - \alpha+\alpha$ |
| | 202E | 5F | MOV E,A | ADDRESS OF DELAY WORD FOR $\alpha$ i.e. $222\alpha$ |
| | 202F | 16 22 | MVI D,22 | |
| | 2031 | 1A | LDAX D | LSB OF DELAY WORD IN COUNTER 2 |
| | 2032 | D3 12 | OUT 12 | |
| | 2034 | 13 | INX D | |
| | 2035 | 1A | LDAX D | MSB OF DELAY WORD IN COUNTER 2 |
| | 2036 | D3 12 | OUT 12 | |
| | 2038 | DB 0A | IN 0A | STATUS OF QUANTIZER |
| | 203A | E6 07 | ANI 07 | MASK HIGHER 5 BITS |
| | 203C | 86 | ADD M | COMPUTE ADDRESS OF FIRING COMMAND WORD |
| | 203D | 4F | MOV C,A | |
| | 203E | 23 | INX H | STATUS OF $3\phi$ LINE VOLTAGE + POINTER |
| | 203F | 66 | MOV H,M | |

| LEBEL | ADDRESS | CONTENTS | MNEMONICS AND OPERANDS | COMMENTS |
|---|---|---|---|---|
| | 2040 | 69 | MOV L,C | |
| | 2041 | 00 | NOP | |
| | 2042 | 3E 0D | MVI A, 0D | UNMASK RST 6.5 |
| | 2044 | 30 | SIM | |
| | 2045 | FB | EI | |
| | 2046 | 76 | HLT | SYN.WITH RST 6.5 |
| | 2047 | C9 | RET | RET FROM RST 6.5 |
| | 2048 | 00 | NOP | |
| | 2049 | 00 | NOP | |
| ISS.RST 6.5 | 204A | 7E | MOV A,M | SCR PAIR SELECTED |
| | 204B | D3 08 | OUT 08 | |
| | 204D | 3E A0 | MVI A, A0 | DELAY=PULSE WIDTH |
| | 204F | 3D | DCR A | |
| | 2050 | C2 4F 20 | JNZ 204F | |
| | 2053 | AF | XRA | TERMINATE 0PULSE |
| | 2054 | D3 08 | OUT 08 | |
| | 2056 | 00 | NOP | |
| | 2057 | 00 | NOP | |
| | 2058 | 00 | NOP | |
| | 2059 | C9 | RET | |

PH OF EXPERIMENTAL SET UP